

Response to the Editor

P. R. Lindgren et al.

Comment on “Detecting methane ebullition on thermokarst lake ice using high resolution optical aerial imagery”

Thank you very much for giving the time to read the manuscript and for providing very valuable feedback. We have revised our manuscript based on the comments. And below are (1) our response to all the comments, (2) a list of all relevant changes made in the manuscript, and (3) the marked-up manuscript.

Comments

1. Page 1 Line 5: Is this necessary?

We agree. It is not necessary to use ‘bubbling’ here in the extract. Therefore, we have removed it.

2. Page 1 Line 8-9: This is unclear (because you are using both “as a function” and “versus” and “as” in the same sentence!). And why “versus time” if the image is a snap shot in time?

We have reworded the sentence for clarity. “Bubbles impeded by the lake ice sheet in winter form distinct white patches as a function of ebullition rate when lake ice grows down and around them”.

3. Page 1 Line 16: Replace by “this”?

We have replaced “our” by “this”

4. Page 1 Line 25-27: Why the distinction between the last 2?

We revised this sentence to clarify that the former Pliocene aged sediments are undisturbed, whereas the later were subject to thaw and diagenesis beneath lakes and later refroze once the lakes drained.

5. Page 1 Line 27: Why “however”?

We used “however” here to highlight the vulnerability of permafrost stored soil carbon to permafrost degradation. This is not necessary. So, we have removed it in the revised manuscript.

6. Page 3 Line 17: not necessary, ebullition is comprehensive enough; why mentioning this synonym?

We mentioned “bubbling” here because we use “bubbling” instead of “ebullition” in some parts of the paper. We think this is important so that the casual readers are not confused.

7. Page 4 Line 2: This standard deviation (and the other below for other types) corresponds to which data set? How many lakes? How many measurements? Over what region? For what type of permafrost and sediment deposits? This is not a generality

We have now provided further details on the ebullition rates reported in the paper.

“They identified four major types of methane ebullition seeps based on ice bubble cluster morphology and they measured daily mean ebullition rates (Fig. 1) (Walter Anthony and Anthony, 2013). It should be noted that seep class-specific ebullition rates reported represent the daily average of thousands of flux measurements measured on 24 panarctic lakes in continuous and discontinuous permafrost region for up to 700 days; however, bubbling within each class is highly episodic, and bubbling rates of individual seeps are not constant over time

8. Page 4 Line 23: I suggest to replace "variability of ebullition bubbles" by "whole-lake ebullition" to clarify this sentence. And just an idea to make the text lighter: "ebullition bubble" seems a redundant expression, which is repeated at several occasions throughout the paper. I understand that bubbles formed by ice exclusion of gases are not coming from sediment ebullition, but is this the only reason why you keep using this expression throuhout? I think readers can understand that when you talk about bubbles, you are referring to ebullition bubbles.

We appreciate your feedback. Here “variability of ebullition bubbles” implies variability of ebullition in space and time, which we have discussed in the preceding lines. We are trying to convey that if the spatial and temporal variability of ebullition is not taken into account then it leads to less accurate estimation of methane flux at larger spatial scales.

We agree “ebullition bubble” seems redundant but we think it is important to use the expression throughout the text to maintain the distinction of ebullition type bubble from other types.

9. Page 5 Line 8-9: Why is gas dissolved in water affecting ice backscattering properties caused by bubbles trapped in ice? Is this only affecting the properties of the bottom of

ice cover (late winter), but that can also be seen with SAR?

Our intention is to inform the readers about the time of the year when dissolved gas concentration in lake water are highest. It is the gas bubbles trapped in lake ice that affect SAR backscattering properties, not the dissolved gas in lake water. We have removed the discussion of SAR backscatter properties of non-ebullition bubbles trapped in lake ice to shorten this section. Please see the reply below, #10.

10. Page 5 Line 12: Why starting the sentence “in contrast” then?

We have removed lines 2-12 to keep this section concise and clear, also as per your suggestion (comment # 12). We decided to remove this section that discussed the detection of tiny non-ebullition gas bubbles since it is not very relevant in our study. In the revised manuscript, we only highlight the previous studies by Walter et al. (2008) and Engram et al. (2012) that successfully used SAR to detect ebullition bubbles.

11. Page 5 Line 18: is this necessary?

We want readers to be clear that Walter Anthony et al. (2012) also relied on aerial photographs in addition to their observations during the flights to map open-water holes in lake ice.

12. Page 5: I suggest to make sure all these considerations are important to the introduction because it is a little long now.

Thank you for your feedback. We have shortened this section and highlighted only the important sections that are relevant to our study. Please, see response # 10.

13. Page 16, Line 4: larger?

We have replaced ‘large’ with ‘larger’.

14. Page 16, Line 5-6: done on what year? Both?

Field-based estimate of whole-lake ebullition for Goldstream Lake is from multiple year of data (2007-2011). We have now mentioned it in the revised manuscript.

15. Page 16, Line 12: higher only in 2012

We agree 2012 estimate is much higher. But in both years we find an overestimation of Hotspots. We have discussed this in this paragraph and also in section 4.2 of the revised manuscript. In this paragraph we added – “It is important to note that while the whole-lake methane flux estimates from our aerial survey are close to those based on ground surveys, the flux estimates for individual seep types may vary between the methods. It is also possible that with aerial surveys we are underestimating the total contribution of methane flux from low flux seeps because they had not expressed completely when we acquired our aerial photos and that we are overestimating the contribution from high flux seeps.”

16. Page 17, Line 13: do not?

We have replaced ‘don’t’ with ‘do not’

17. Page 20, Line 26-29: It could be interesting that you mention if these images are expensive (or free)? One could wonder if this is affordable when 100km² is 2-3K (?) for pan-arctic estimations.

We agree this could be useful information. But the cost of aerial surveys and images depends on vendors. It can also vary from one place to another. Therefore, we cannot tell exactly how affordable this is.

18. Page 22, Line 17: any indications from boreal lakes for ex. that this type of ebullition is occurring? (seeps and hotspots)

Seep ebullition is known to occur in both tundra and boreal lakes (Walter Anthony and Anthony 2013, JGR Biogeoscience). In fact, Goldstream Lake is a boreal thermokarst lake. For clarity, we have added the phrase, "...in tundra and boreal zones". The sentence now reads, "Our approach is applicable to other regions and will help to characterize methane ebullition emissions from seasonally ice-covered lakes, including thermokarst and non-thermokarst lakes in tundra and boreal zones."

19. Reviewer’s comment, Page 3: It is not clear what you have done about this comment in the revised ms

Since ice growth does not have major implications in our study, we decided not to discuss this in the paper to keep it concise.

20. Reviewer’s comment, Page 4: There seems to be 3 types of sources associated to a hole in the ice: hotspots, groundwater springs, and geologic seepage, right? It is not clear what you have done about this comment in the revised ms.

We agree. There are various sources associated to a hole in ice. Ground water springs and geologic seepage aren’t extensive and are found in only small fraction of water bodies and also we do not encounter this issue in our study. Therefore, we decided not discuss this in detail in the paper to keep it concise and avoid confusions. But we did mention the distinction of geologic methane seeps from Hotspots in the Introduction, paragraph 5. "..., photograph,

and map large ($\sim 1 \text{ m}^2$ to $> 300 \text{ m}^2$) bubbling-induced open-water holes in ice-covered lakes in Alaska associated with geologic methane seepage. *Geologic methane seeps differ distinctly from ecological Hotspots in associated fluxes (i.e. geologic seeps are several orders of magnitude higher flux than Hotspots) and spatial distribution.* ... this study showed that geologic methane seepage is not extensive, but it is important in some regions of Alaska underlain by leaky hydrocarbon reservoirs.”

21. Reviewer’s comment, Page 4: Does it also imply non-yedoma lakes have no hotspots?

It does not imply non-yedoma lakes have no Hotspots, but Hotspots are more rare in non-yedoma lakes. Radiocarbon dating of seep bubbles in yedoma lakes showed that Hotspot ebullition originates from deep within the thaw bulb where organic carbon is made available to microbial decomposition by new permafrost thaw at depth in sediments. In non-yedoma lakes, organic substrates are typically supplied to lakes in shallower sediments, forming seeps with lower flux rates.

22. Reviewer’s comment, Page 12: I think inversely needs to be removed to clarify the sentence

Thank you for your feedback. We have removed ‘inversely’.

23. Reviewer’s comment, Page 13: is this avenue mentioned in discussion?

We have mentioned this in section 4.5, paragraph 4, in the revised manuscript. “... variable during our study period compared to low-flux A- and B-type seeps. However, long-term remote sensing and ground-based observations are required to further test our hypothesis of seep regularity that high flux seeps are temporally more stable in their location than low flux seeps. Additionally, long-term data may also help to account for the difference in pressure and look at possible changes in seep type over the years.”

Major Changes

I. Changes in title and sections

1. We changed the title of the manuscript. The title now reads, “Detection and Spatio-Temporal Analysis of Methane Ebullition on Thermokarst Lake Ice Using High Resolution Optical Aerial Imagery”.
2. Methods, section 3, reorganized for clarity.
Methods section starts with a short summary. It is subdivided into the following sections.
 - 3.1 Remotely sensed high-resolution image acquisition
 - 3.2 Ground truth field data
 - 3.2.1 Fall 2011 and 2012 field surveys
 - 3.2.2 Spring 2011 and 2012 field surveys
 - 3.2.3 Spring 2013 field surveys
 - 3.3 Mapping ebullition seeps on lake ice
 - 3.3.1 Pre-processing of images

- 3.3.2 Identification of bubble patches on snow-free lake ice
 - 3.3.3 Identification of open-hole Hotspots on snow-covered lake ice
 - 3.4 Statistical analysis
 - 3.4.1 Interpretation of image data results
 - 3.4.2 Classification of bubble patches
 - 3.4.3 Analysis of spatial distribution of bubble patches
 - 3.4.4 Analysis of temporal pattern of bubble patches
- 3. Results and Discussion, section 4, reorganized for clarity.
 - 4.1 Relationship between bubble patch brightness and field-measured methane flux
 - 4.2 Classification of bubble patches
 - 4.3 Estimation of whole-lake methane flux
 - 4.4 Spatial distribution of bubble patches in relation to thermokarst lake
 - 4.5 Multi-year comparison of bubble patch characteristics: 2011 and 2012
- 4. We shortened the Conclusion.

II. Addition and removal of texts

- 5. We have included the relative merits of optical aerial image analysis and the SAR techniques in section 5 'Benefits and challenges of aerial image analysis for ebullition seep mapping'. We have re-arranged the paragraphs too. The section starts with benefits of optical remote sensing.
- 6. We removed Tiny-type seep from Methods section and only mentioned it in the results and discussion, section 4.1.
- 7. We have moved some technical remote sensing portions of methods in the revised manuscript to the supplementary section to keep it concise for clarity. We have now provided the technical details on Principal Component Analysis (PCA), object-based segmentation and classification, and classification of bubble patches as supplemental text.

III. Changes in figures, tables and supplemental materials

- 8. We have reversed the PC 1 values in figures 2 and 3 (i.e. dark pixels/low DN values in PC 1 component is less bright bubbles and bright pixels/high DN values is brighter bubbles). We have explained this in Methods section 3.4.1 and provided supplementary material for more detail.
- 9. We have provided the regression equations and RMSE for the relationship between bubble patch percent coverage and distance from thermokarst shore in Figure 5.
- 10. We have added more detail in Figure 8 caption for clarity and shortened the graph detail in the main text (section 4.5).
- 11. We removed Table 2 in the revised manuscript.
- 12. We have added more texts, figures and tables in Supplementary section.

**Detection and Spatio-Temporal Analysis of Methane
Ebullition on Thermokarst Lake Ice Using High Resolution
Optical Aerial Imagery**

P. R. Lindgren¹, G. Grosse^{2,1}, K. M. Walter Anthony³, F. J. Meyer¹

[1] Geophysical Institute, University of Alaska Fairbanks, USA

[2] Alfred Wegener Institute Helmholtz Centre for Polar and Marine Research, Potsdam,
Germany

[3] Water and Environmental Research Center, University of Alaska Fairbanks

Correspondence to: P. R. Lindgren (pregmi@alaska.edu)

Abstract

Prajna Lindgren 9/19/15 11:28 PM

Deleted: ng

1 Thermokarst lakes are important emitters of methane, a potent greenhouse gas. However,
2 accurate estimation of methane flux from thermokarst lakes is difficult due to their
3 remoteness and observational challenges associated with the heterogeneous nature of
4 ebullition. We used high-resolution (9 -11 cm) snow-free aerial images of an interior Alaskan
5 thermokarst lake acquired 2 and 4 days following freeze-up in 2011 and 2012, respectively, to
6 detect and characterize methane ebullition seeps and to estimate whole-lake ebullition.
7 Bubbles impeded by the lake ice sheet form distinct white patches as a function of bubbling
8 when lake ice grows down and around them. Our aerial imagery thus captured a snapshot of
9 bubbles trapped in lake ice during the ebullition events that occurred before the image
10 acquisition. Image analysis showed that low-flux A- and B-type seeps are associated with low
11 brightness patches and are statistically distinct from high-flux C-type and Hotspot seeps
12 associated with high brightness patches. Mean whole-lake ebullition based on optical image
13 analysis in combination with bubble-trap flux measurements was estimated to be 174 ± 28 ml
14 gas $m^{-2} d^{-1}$ and 216 ± 33 ml gas $m^{-2} d^{-1}$ for the years 2011 and 2012, respectively. A large
15 number of seeps demonstrated spatio-temporal stability over our two-year study period. A
16 strong inverse exponential relationship ($R^2 \geq 0.79$) was found between percent surface area
17 of lake ice covered with bubble patches and distance from the active thermokarst lake margin.
18 Even though the narrow timing of optical image acquisition is a critical factor, with respect to
19 both atmospheric pressure changes and snow/no-snow conditions during early lake freeze up,
20 our study shows that optical remote sensing is a powerful tool to map ebullition seeps on lake
21 ice, to identify their relative strength of ebullition and to assess their spatio-temporal
22 variability.

23

24 1 Introduction

25 Soils in the northern permafrost region contain 1300-1370 Pg of organic carbon with an
26 uncertainty range of 930-1690 Pg (Hugelius et al., 2014). A large amount of soil carbon in the
27 Yedoma permafrost region (~450 Pg) is found in thick Holocene deposits in thermokarst lakes
28 and basins, undisturbed Pleistocene-age ice-rich silts known as yedoma, and Pleistocene
29 deposits thawed underneath lakes and later refrozen (Grosse et al., 2011; Walter Anthony et
30 al., 2014). Permafrost degradation can facilitate the transfer of this permafrost stored carbon
31 to the atmosphere in the form of the greenhouse gases carbon dioxide (CO₂) and methane
32 (CH₄), resulting in a positive feedback to global climate change (Zimov et al., 2006; Walter et

Prajna Lindgren 11/7/15 7:48 AM

Deleted: (bubbling)

Prajna Lindgren 9/4/15 10:59 AM

Deleted: multi-temporal

Prajna Lindgren 9/4/15 2:43 PM

Deleted: , Goldstream Lake,

Prajna Lindgren 11/7/15 7:49 AM

Deleted: rate versus time as

Prajna Lindgren 11/7/15 7:49 AM

Deleted: thickens

Prajna Lindgren 9/4/15 2:42 PM

Deleted: in a single

Prajna Lindgren 9/6/15 10:55 PM

Deleted: 0

Prajna Lindgren 9/6/15 10:49 PM

Deleted:

Prajna Lindgren 11/11/15 10:50 AM

Deleted: However, p

al., 2006; Schuur et al., 2008; Koven et al., 2011). One common and effective form of permafrost degradation involves formation and growth of thermokarst lakes (Grosse et al., 2013; Kokelj and Jorgenson, 2013), which tap into deep (up to 60m) permafrost carbon pools (Zimov et al., 1997; Walter et al., 2008a).

Thermokarst lakes are a prominent landscape feature in the high northern latitudes (Smith et al., 2007; Grosse et al., 2013). They are formed in closed depressions following the thawing of ice-rich permafrost or melting of massive ice. Once initiated, the presence of a water body on permafrost serves as a positive feedback to permafrost degradation. Depending on the amount of excess ice content in permafrost, this positive feedback accelerates the growth of thermokarst lakes in both lateral and vertical directions (Jorgenson and Shur, 2007; Plug and West, 2009; Kokelj and Jorgenson, 2013). Over many years, taliks (thaw bulbs) of perennially thawed soil develop beneath thermokarst lakes (Hinzman et al., 2005; West and Plug, 2008; Rowland et al., 2011) creating conditions favorable for year-round methane production through anaerobic decomposition of organic matter by microbes (Zimov et al., 1997; Walter et al., 2006, 2008a; Kessler et al., 2012). During lateral expansion, thermal erosion along the lake margin also releases both Holocene and Pleistocene organic matter from adjacent soils into anaerobic lake bottoms further enhancing methanogenesis (Zimov et al., 1997; Walter Anthony et al., 2014).

Ebullition (bubbling) is considered the dominant pathway of methane release from lakes to the atmosphere (Keller and Stallard, 1994; Bastviken et al., 2011). Methane produced in dense lake sediments and thaw bulbs emerges primarily through intrasedimentary bubble tubes as point-source seeps on the lake bed (Walter Anthony et al., 2010). In the high northern latitude region, where lake surfaces freeze throughout the winter, most bubbles emerging from the lake bed ascend through the water column and get trapped by ice as gas-pockets (Walter et al., 2008b; Greene et al., 2014). Ongoing ice growth can separate ice-trapped bubbles from an individual seep by thin films of ice, resulting in vertically oriented bubble columns in the ice. Walter et al. (2006) took advantage of this phenomenon to reveal locations and relative strength of “point-sources” of methane seep ebullition across lake ice. They identified four major types of methane ebullition seeps based on ice bubble cluster morphology and they measured daily mean ebullition rates ($\text{mean} \pm \text{standard error of mean}$) (Fig. 1) (Walter Anthony and Anthony, 2013). It should be noted that the seep class-specific ebullition rates reported represent the daily average of thousands of flux measured on 24

1 | panarctic lakes in continuous and discontinuous permafrost region for up to 700 days;;
2 | however, bubbling within each class is highly episodic, and bubbling rates of individual seeps
3 | are not constant over time (Walter Anthony et al., 2010; Walter Anthony and Anthony, 2013):
4 | (1) A-type seeps are characterized by isolated bubbles stacked in multiple vertical layers with
5 | less than 50% of all gas volume merged in bubble clusters. A-type seeps have the lowest
6 | ebullition rate (22 ± 4 ml gas d⁻¹); (2) B-type seeps are dominated by laterally-merged
7 | bubbles stacked in multiple layers (more than 50% of all gas volume merged in a bubble
8 | cluster). The ebullition rate of this bubble type is 211 ± 39 ml gas d⁻¹; (3) C-type seeps,
9 | associated with an ebullition rate of 1726 ± 685 ml gas d⁻¹, are characterized by single large
10 | gas pockets (usually > 40 cm in diameter) separated vertically by ice layers containing few or
11 | no bubbles; and (4) Hotspot seeps have the highest ebullition rate, on average 7801 ± 764 ml
12 | gas d⁻¹. Due to upwelling of water associated with frequent bubble streams, Hotspots
13 | generally appear as open-water holes in lake ice following freeze up. Usually a thin snow-ice
14 | film develops over Hotspots in winter, visually masking them at the surface; however, ice
15 | blocks cut from the lake throughout winter and spring reveal that Hotspot bubbling maintains
16 | a large ice-free cavity throughout winter (Greene et al., 2014).

17 | Accounting for methane ebullition from northern thermokarst lakes can significantly improve
18 | estimates of lake contributions to regional and global atmospheric carbon budgets (Walter et
19 | al., 2007; Bastviken et al., 2011). However, due to challenges associated with the logistics of
20 | fieldwork in remote locations as well as spatial and temporal heterogeneity of ebullition,
21 | accurate estimation of methane flux from thermokarst lakes is difficult (Casper et al., 2000;
22 | Bastviken et al. 2004; Wik et al., 2011). Most studies have been carried out using field
23 | measurements to understand the spatial and temporal variability of methane ebullition.
24 | However, insufficient field data is a recurring issue since it is difficult to sample the entire
25 | lake area, particularly when lakes have remote locations. This may lead to an unrealistic
26 | characterization of variability of ebullition bubbles and a less accurate estimation of methane
27 | flux at a regional scale. Recently, Walter Anthony and Anthony (2013) combined point-
28 | process modeling with field-measured data to understand the drivers of ebullition spatial
29 | variability in thermokarst lakes and provided ways to reduce uncertainty in regional-scale lake
30 | ebullition estimates based on limited field data; nonetheless spatially-limited field sampling
31 | remains a hindrance to whole-lake ebullition quantification.

Prajna Lindgren 11/11/15 9:12 AM

Deleted: ments

Prajna Lindgren 9/6/15 10:54 PM

Deleted:

Remote sensing methods combined with field observations can help overcome some of the limitations that exist in a sole field-survey method. One of the major advantages of remote sensing tools is that they may provide the possibility to map the entire population of methane ebullition bubbles on a lake. Moreover, remote sensing can overcome the logistical difficulties that exist in accessing methane-bubbling lakes in the remote regions of the Arctic and Subarctic. Walter et al. (2008b) and Engram et al. (2012) demonstrated the potential application of SAR satellite imagery to estimate whole-lake ebullition from spatially-limited field measurements of ebullition along survey transects. These studies showed correlation of radar backscatter values with the percent surface area of lake ice covered with bubbles and field-measured methane ebullition rates based on bubble-trap measurements from lakes. Additionally, Walter Anthony et al. (2012) used aerial surveys to identify, photograph, and map large (~1 m² to > 300 m²) bubbling-induced open-water holes in ice-covered lakes in Alaska associated with geologic methane seepage. Geologic methane seeps differ distinctly from ecological Hotspots in associated fluxes (i.e. geologic seeps are several orders of magnitude higher flux than Hotspots) and spatial distribution. Coupling aerial surveys with ground truth flux measurements and laboratory analyses, this study showed that geologic methane seepage is not extensive, but it is important in some regions of Alaska underlain by leaky hydrocarbon reservoirs.

Since open holes in snow covered lake ice induced by bubbling are visually distinct, and since lower-flux ebullition bubble clusters trapped inside ice appear as bright white features that have a strong contrast against dark, bubble-free congelation snow free ice (Fig. 1), there is the potential and need to detect and quantify methane bubbles with optical remote sensing. In this study, we explored high-resolution optical remote sensing images to characterize methane ebullition seeps on Goldstream Lake, an interior Alaska thermokarst lake, and study their spatio-temporal dynamics.

2 Study Site

Goldstream L. (64.91°N, 147.84°W; 195 m asl) is an interior Alaska thermokarst lake covering an area of approximately 10,300 m² with maximum and average depths of 2.9 m and 1.6 m, respectively. The lake formed in 'yedoma-type' deposits of retransported late-Quaternary loess at the toe slope of Goldstream Valley in Fairbanks (Péwé, 1975; Kanevskiy et al., 2011; Walter Anthony and Anthony, 2013). Based on remotely-sensed aerial and

Prajna Lindgren 11/11/15 9:14 AM

Deleted: Previously, scientists who used remotely sensed images from synthetic aperture radar (SAR) sensors to study lake ice phenology detected tiny (1-5 mm diameter) vertically-oriented tubular gas bubbles trapped in ice that form when dissolved gases are excluded during ice formation (Jeffries et al., 1994; Jeffries et al., 2005; Duguay et al., 2003). The presence of these sometimes densely-packed non-ebullition gas bubbles, which are usually ubiquitous across the lake if they occur in the ice at all (Boereboom et al., 2012), can have significant effect on spectral and SAR backscatter properties of lake ice, particularly in late winter and spring when dissolved gas concentrations in lake water are highest (Phelps et al., 1998; Langer et al., 2014). In contrast, individual ebullition bubbles, which are larger (0.5-3 cm) (Walter Anthony et al., 2010; Langer et al., 2014) and tend to cluster together (cluster diameter usually 5 to >100 cm), are also detected with remote-sensing SAR sensors (Engram et al., 2012).

Prajna Lindgren 11/7/15 7:19 AM

Deleted:

Prajna Lindgren 9/5/15 11:32 PM

Deleted:

Prajna Lindgren 9/5/15 11:32 PM

Deleted: study methane ebullition at

Prajna Lindgren 9/4/15 11:10 AM

Deleted: (Fig. 1). We first mapped ebullition bubbles trapped in early winter lake ice in aerial images. We refer to the bubble features seen in our images as 'bubble patches' henceforth since the image resolution was not sufficient to fully resolve small individual bubbles (Fig. 1). Then we characterized imaged bubble patches based on field-based ebullition bubble seep data collected approximately 1-2 weeks after image acquisition in the fall of 2011 and 2012 and again in spring of the following year. We hypothesized that the brightness of bubble patches correlates with the strength of methane flux associated with four classes of ebullition bubble seeps (A, B, C and Hotspot) identified by Walter Anthony et al. (2010). We estimated from aerial photos the bubble patch density for each seep class as well as the mean whole-lake seep ebullition, examined the spatial patterns of seep locations in the lake with respect to eroding thermokarst shores, and analyzed spatio-temporal variability of seep occurrences by comparing imagery from different years.

Prajna Lindgren 9/8/15 3:46 PM

Deleted:

Prajna Lindgren 9/8/15 3:51 PM

Deleted: ear

satellite images, the lake partially drained between 1949 and 1978 but has been expanding mainly along the eastern shore since then (Fig. 1f). This active thermokarst expansion is also indicated by spruce trees leaning lake-ward along the eastern lake margin, and standing dead trees submerged in the lake offshore of the eastern margin. The vegetation around the lake is dominated by black spruce and willow. Cattail (*Typha* spp.) grows along some shallow margins of the lake. Water lilies (*Nuphar* spp.) are also found in several locations on the northern and south-western parts of the lake.

Ebullition accounts for total of 83% of methane emission from Goldstream L. (Greene et al., 2014). The concentration of methane in Goldstream L.'s bubbles is 82-89% (Greene et al., 2014). Ice formation on the lake usually occurs between the end of September to mid-October, reaches maximum thickness by mid-March, and ice break up occurs around the end of April or early May. Vertically oriented layers of methane ebullition bubbles (Fig. 1), representing point-source seeps, are widespread in the lake ice particularly along the eastern margin (Walter Anthony and Anthony, 2013). Many Hotspot seeps are also found near the eastern eroding shore and are seen as open holes in lake ice during early winter and spring.

3 Methods

We used three sets of data in our study: (1) high-resolution snow-free early winter lake ice images from fall 2011 and 2012 (2) high-resolution snow-covered early winter lake images from fall 2012 and (3) field-based ebullition bubble seep types and their fluxes.

We first mapped ebullition bubbles trapped in early winter lake ice in snow-free aerial images after we processed the images acquired in the fall of 2011 and 2012. We refer to the bubble features seen in our snow-free images as 'bubble patches' henceforth since the image resolution was not sufficient to fully resolve small individual bubbles (Fig. 1). Then we characterized imaged bubble patches based on field-collected ebullition bubble seep data collected approximately 1-2 weeks after image acquisition when ice was safe to walk on in the fall of 2011 and 2012 and again in spring of the following year. We hypothesized that the brightness of bubble patches correlates with the strength of methane flux associated with four classes of ebullition bubble seeps (A, B, C and Hotspot) identified by Walter Anthony et al. (2010). We estimated from aerial photos the bubble patch density for each seep class and the mean whole-lake seep ebullition. Finally, we examined the spatial patterns of seep locations

Prajna Lindgren 9/19/15 10:56 PM

Deleted: years

Prajna Lindgren 9/25/15 8:59 AM

Deleted: Goldstream L.

in the lake with respect to eroding thermokarst shores, and analyzed interannual variability of seep occurrences by comparing imagery from different years.

Due to similar spectral characteristics of open water and dark lake ice, open-hole Hotspots are difficult to map on snow-free lake ice image. But they are easily identifiable on snow-covered lake ice image. Therefore, we also collected high-resolution snow-covered aerial images in the fall of 2012 to map open-hole Hotspots on the lake. We compared the locations of Hotspots in aerial images with maps of Hotspot locations determined by field measurements over multiple years to assess Hotspot regularity.

3.1 Remotely sensed high-resolution image acquisition

We scheduled low altitude, high-resolution aerial image acquisitions to map and characterize methane ebullition bubble patches (A, B, C and ice-covered Hotspots) during a narrow time window in the early winter, when first ice had formed but was still snow-free. Images were acquired in nadir with a Navion L17a plane using a Nikon D300 camera system mounted in a bellyport on 14 October 2011 and 13 October 2012, two and four days following freeze-up, respectively. Flight altitude for the acquisitions was ~750 m asl in 2011 and ~587 m asl in 2012. Image scale was 1:20,000 and 1:17,000 for 2011 and 2012, respectively which in turn corresponds to ground sampling distances (GSD) of 11 cm and 9 cm.

We collected images of the snow-covered lake in fall 14 October 2012 using an Unmanned Aerial Vehicle (UAV) mounted with an Aptina MT9P031 board camera to map open-hole Hotspot seep locations. The images were acquired from a flying height of approximately 230 m asl, corresponding to an image scale 1:30,000 and GSD of 6 cm. All the images consisted of three visible bands: red, green and blue (RGB).

3.2 Ground truth field data

We collected the point location data of (1) the lake perimeter and permanently installed reference markers as Ground Control Points (GCPs) to perform rectification of aerial images and (2) methane ebullition seeps on Goldstream L. in the fall and spring of 2011 and 2012 using a survey-grade LEICA VIVA™ real time kinematic Differential Global Positioning System (DGPS) with centimeter-accuracy.

3.2.1 Fall 2011 and 2012 field surveys

Prajna Lindgren 9/4/15 11:27 AM

Deleted: <#>Ground truth field data - ... [1]

Prajna Lindgren 9/8/15 8:32 PM

Deleted: bubbles

Prajna Lindgren 8/24/15 12:59 PM

Deleted: respectively

Prajna Lindgren 9/8/15 7:52 PM

Deleted: Additionally, we

Prajna Lindgren 9/8/15 8:38 PM

Deleted: ice-free

We surveyed the lake perimeter and measured several permanently installed reference markers. We conducted detailed ebullition ice-bubble surveys in October 2011 two weeks after image acquisition when lake ice was safe to walk on. The surveys were performed within two large polygons that are identified in Fig. 1f: One about ~ 7 m from the eastern thermokarst shore and a second near the center of the lake. The surveyed polygons in the east and center of the lake covered ~ 428 m² and ~ 236 m², respectively, and were reported in detail in Walter Anthony and Anthony (2013) and Greene et al. (2014).

In October 2012, we performed bubble surveys 6 days after image acquisition in three other polygons (total area ~ 200 m²) randomly distributed across the lake (Fig. 1f). We performed bubble surveys earlier after image acquisition than in 2011 to avoid white ice condition. We used the seep identification method described by Walter Anthony et al. (2010)

3.2.2 Spring 2011 and 2012 field surveys

While field-based estimations of A, B, and C-type seeps were limited to survey plots covering about 13 % of the lake area, the locations of Hotspot seeps were mapped across the whole lake using detailed DGPS surveys of open holes in October and April 2011 and 2012. Hotspots were detected visually at these times of the year as open-water holes in lake ice.

3.2.3 Spring 2013 field surveys

In April 2013, we extracted several blocks of the full lake-ice column at seep locations to investigate the temporal ebullition patterns that developed throughout the winter season.

3.3 Mapping ebullition seeps on lake ice

3.3.1 Pre-processing of images

We conducted the following image pre-processing: (1) We performed mosaicking of multiple images of Goldstream L. to construct a complete image of the lake. This was achieved by using Agisoft PhotoScan Professional Software™ Version 0.9.0. (2) We then performed geometric image rectification with 22 DGPS-collected GCPs using a second order polynomial transformation with bilinear resampling. The GCPs were distributed mostly around the lake perimeter. Some of them were identifiable reference points on the lake such as cattail vegetation and LiCor methane analyzer installed on the lake; (3) For image enhancement we applied a feature linear transformation on all three visible spectral bands of the lake images using unstandardized Principal Component Analysis (PCA). Both geometric and spectral

Prajna Lindgren 9/8/15 8:20 PM
Deleted: bubble patches in early winter snow-free lake ice images

Prajna Lindgren 9/4/15 11:42 AM
Deleted: initially performed

Prajna Lindgren 9/23/15 4:03 PM
Deleted: .

Prajna Lindgren 9/19/15 10:59 PM
Deleted: bilinear

Prajna Lindgren 9/23/15 4:04 PM
Deleted: Finally, f

image transformations were performed in ENVI™ image processing software, Version 4.8. PCA spectral transformation produced three independent principal component (PC) bands. The first band (PC 1 band) consisted of the variables that explained the most variance (> 98%) in the dataset attributing to bubble patches (Fig. 2, Supplement Text S1).

3.3.2 Identification of bubble patches on snow-free lake ice

We applied a classification technique based on object-based image analysis (OBIA) to semi-automatically identify and map methane ebullition bubble patches in the PCA-transformed images using eCognition Developer™ 8 (Lindgren et al. in prep). Our object-based classification method comprises of two steps: (1) image segmentation, i.e. aggregation of homogenous image pixels based on their spatial and spectral homogeneity into meaningful clusters known as image objects, and (2) classification of image objects (Navulur, 2007; Blaschke and Strobl, 2001). Varying ice conditions on the lake such as (a) clear, dark congelation ice, (b) milky white snow-ice, and (c) ice with shadows from neighboring trees added challenges to identifying ebullition bubble patches. We were able to resolve these challenges by integrating semantic information associated with image objects in classification (Lindgren et al. in prep). For this, the scene is first decomposed into meaningful regions that represent different areas of lakes such as vegetation, shadow, dark, and white ice. These regions are then organized in a conceptual image object hierarchy creating a semantic network between different sized image objects; large-scale objects in the upper level called super objects and small-scale objects in the lower level called sub-objects (Supplement Fig. S1; Lindgren et al. in prep). For example, the lake area is a super-object composed of sub-objects associated with various lake ice characteristics (e.g. shadow, dark black ice) whereas areas of specific lake ice characteristics are super-objects of our final target feature, ebullition bubble patches. At each level, image segmentation and classification are performed to delineate and label target regions. For example in the first level, segmentation is performed on the whole lake image to identify lake shore and lake. In the second level, only the lake region is segmented and image objects derived from the lake are classified into different lake ice characteristics. The process continued as it proceeded towards lower and finer classification levels until bubble patches were identified in the lake ice in the final stage. This approach of detecting image objects from coarser to finer scale has been described as an effective way to classify images in OBIA (Blaschke et al., 2008).

Prajna Lindgren 9/23/15 4:04 PM

Deleted: Multi-spectral remote sensing data consists of high inter-band correlation and therefore bands within a dataset carry redundant information (Rocchini et al., 2007). PCA transforms a set of correlated variables (original bands) into a set of linearly uncorrelated orthogonal components (principal components) (Schowengerdt, 2007; Estroñell et al., 2013). It reduces the dimensionality of the data and outputs the maximum amount of information with a physical meaning from the original bands into the least number of principal components (Estroñell et al., 2013). After transformation, the first principal component has the variables that account for the most variance in the dataset and each succeeding independent component in turn carries less and less of the original data variance. In our case, the first PC band (PC 1) carried the most variance (> 98%) attributing to bubble patches (Fig. 2). Visually, bubble patches on the lake ice appeared as dark patches in PC 1 band with low PC 1 grey values and were quite distinct from the surrounding lake ice.

Prajna Lindgren 9/4/15 11:43 AM

Deleted: then

Prajna Lindgren 9/23/15 4:12 PM

Deleted: d

Prajna Lindgren 9/23/15 4:17 PM

Deleted: we first decomposed our

Prajna Lindgren 9/23/15 4:18 PM

Deleted: We

Prajna Lindgren 9/23/15 4:18 PM

Deleted: then organized

Prajna Lindgren 9/23/15 4:18 PM

Deleted: them

Prajna Lindgren 9/9/15 11:55 PM

Deleted: i

Prajna Lindgren 9/4/15 4:09 PM

Deleted: different

Prajna Lindgren 9/23/15 4:05 PM

Deleted: In

Prajna Lindgren 9/4/15 11:48 AM

Deleted: object

Prajna Lindgren 9/4/15 11:48 AM

Deleted: image objects within the boundary of super-objects were altered and refined through merging and segmentation to form sub-objects with 1:n relationship between super- and sub-object. At an early stage, we applied coarser

Prajna Lindgren 9/4/15 11:48 AM

Deleted: (i.e. broad scale segmentation)

Prajna Lindgren 9/4/15 11:48 AM

Deleted: coarser

Prajna Lindgren 9/4/15 11:48 AM

Deleted: . Then in the later stages, finer segmentation (i.e. fine scale segmentation) and classification was performed to delineate and label finer target regions

More information on this hierarchical approach of bubble patch identification can be found in the supplement text (Supplement Text S2) and in Lindgren et al. (in prep).

3.3.3 Identification of open-hole Hotspots on snow-covered lake ice

In images acquired after the first snow fall, hotspots appear dark against the snow-covered lake. Hence, they can be mapped using a simple contrast and split segmentation technique in eCognition Developer™ (eCognition Developer 7 Reference, 2007a). This approach involves choosing a threshold value on the RGB image bands for the algorithm to maximize the contrast between Hotspots and snow-covered lake pixels that separates the image content into dark objects (consisting of pixels below the threshold, i.e. Hotspots) and bright objects (consisting of pixels above the threshold, i.e. snow-covered lake ice).

3.4 Statistical analysis

3.4.1 Interpretation of image data results

We extracted PC 1 grey values of individual ebullition bubble patches mapped in images from the year 2011 and 2012. PC 1 values of image ranged between 0-255. Bubbles patches are visually bright in true color composite (RGB composite) images but appeared darker (i.e. low PC 1 values) than the surrounding lake ice in the PC 1 band (Supplement Fig. S2). Therefore, we inverted PC 1 values of bubble patches to make is visually intuitive, i.e. bubbles that appeared bright in natural color composite also appeared bright in PC 1 band (Fig. 2). Henceforth, we refer to this brightness obtained in inverted PC 1 as PC 1 brightness.

We assessed the relationship of ebullition bubble patch PC 1 brightness values with four distinct types of ebullition seeps that we identified during our field surveys. We performed an analysis of variance (ANOVA) to test the null hypothesis that the mean PC 1 values (and thus true bubble brightnesses via its inverse relationship with the PC 1) of four types of seeps are not significantly different. We applied a post-hoc Tukey's Honest Significant Difference (HSD) test, in case, the null hypothesis was rejected, to identify significantly distinct seeps. Results of this analysis are shown in Section 4.1.

3.4.2 Classification of bubble patches

Prajna Lindgren 9/23/15 4:06 PM

Deleted: Based on empirical performance tests, we used the first two PCA components (PC 1 and PC 2) to perform multi-resolution segmentation embedded in eCognition Developer™ software to create image objects (eCognition Developer 7 Reference, 2007a). The advantage of using multi-resolution segmentation is that it allows to create objects of different scales while minimizing the heterogeneity within the resulting object at the given scale (Baatz and Schape, 2000). For example, we applied a large-scale factor to create objects of different lake ice characteristics and a small-scale factor to create bubble patch objects. We treated regions such as areas of lake ice characteristics independently to perform region-specific classification for the identification of target features within the domain of that particular region. In general, for classification we used spectral characteristics in PC bands 1 and 2, contextual information pertaining to image objects such as an image object's relationship with it ... [2]

Prajna Lindgren 9/8/15 8:40 PM

Deleted: Similarly,

Prajna Lindgren 9/23/15 4:09 PM

Deleted: H

Prajna Lindgren 9/23/15 4:09 PM

Deleted: that

Prajna Lindgren 9/23/15 4:09 PM

Deleted: red

Prajna Lindgren 9/23/15 4:10 PM

Deleted: were mapped

Prajna Lindgren 9/23/15 4:10 PM

Deleted: d

Prajna Lindgren 9/23/15 4:11 PM

Deleted: and separate them

Prajna Lindgren 9/4/15 12:05 PM

Deleted: Interpretation of image ... [3]

Prajna Lindgren 9/8/15 8:45 PM

Deleted:

Prajna Lindgren 9/8/15 8:55 PM

Deleted: natural or

Prajna Lindgren 9/8/15 8:47 PM

Deleted: have low grey values in the PC 1 band

Prajna Lindgren 9/9/15 11:33 PM

Deleted: 2

Prajna Lindgren 9/8/15 8:53 PM

Deleted: A higher brightness of bubble patch ... [4]

Prajna Lindgren 9/8/15 8:19 PM

Deleted:

Prajna Lindgren 9/23/15 2:06 PM

Deleted: proposed to apply

Prajna Lindgren 9/23/15 1:55 PM

Deleted: ly

Prajna Lindgren 9/23/15 2:04 PM

Deleted: T

Prajna Lindgren 9/23/15 2:03 PM

Deleted: (HSD)

Prajna Lindgren 9/23/15 11:09 PM

Deleted: f

We applied a supervised classification using a Maximum Likelihood Classifier (MLC) on the three original visible bands and ~~the extracted PC 1 band~~ to classify mapped bubble patches into four distinct seep classes. The MLC ~~calculates~~ a Bayesian Probability Function from the input training classes and ~~then assigns~~ each pixel in the image to the class ~~of~~ highest membership probability (Mather, 2009). ~~We collected 98 random samples, 35 for training and 63 for validation, on the 2011 image and similarly 181 random samples, 50 for training and 131 for validation, on the 2012 image. The samples were located at seep locations identified using field-collected DGPS data points.~~

~~The MLC approach categorized bubble patches solely based on the pixel spectral characteristics i.e. only using the brightness values of the training samples. Since the size of bubble patches is also an additional important indicator of seep class and methane flux (Walter Anthony et al., 2010), in a subsequent step, we further refined our classification results by integrating size as an additional feature to more accurately assign bubble patches with a seep type (Supplement Text S3, Table S1). Finally, we estimated the seep density and mean whole-lake ebullition rate by assigning the mean long-term flux values for seep types provided by Walter Anthony and Anthony (2013) to our classified bubble patches.~~

3.4.3 Analysis of spatial distribution of bubble patches

We studied the spatial distribution of ebullition bubble patches as a function of distance from the eroding eastern thermokarst shore. For this, we divided the lake area into multiple 5 m wide zones starting from the eastern eroding margin as mapped in a 1949 aerial image (Fig. 1). Lake zones were created on both sides of the 1949 lake margin to cover the present day lake area. We calculated the percent of lake ice area covered with ebullition bubble patches for each zone and then analyzed its relationship to the distance from the eastern shore lines of the lake observed in 1949, 1978 and 2012.

3.4.4 Analysis of temporal pattern of bubble patches

~~We~~ evaluated the multi-temporal (year 2011 and 2012) variability of ebullition bubble patches and assessed their regularities in space and time. We utilized a marked point process model to analyze spatial seep patterns in our multi-year bubble patch dataset derived from the images. Point process modeling was performed on a set of bubble patch centroids with their respective

Prajna Lindgren 9/23/15 11:09 PM

Deleted: their

Prajna Lindgren 9/23/15 11:09 PM

Deleted: component

Prajna Lindgren 9/23/15 11:09 PM

Deleted: estimates

Prajna Lindgren 9/23/15 11:10 PM

Deleted: is then assigned

Prajna Lindgren 9/23/15 11:10 PM

Deleted: with the

Prajna Lindgren 8/26/15 1:57 PM

Deleted: Training

Prajna Lindgren 9/10/15 11:28 PM

Deleted: were collected randomly on the image

Prajna Lindgren 9/10/15 11:28 PM

Deleted: at

Prajna Lindgren 8/24/15 3:20 PM

Deleted: Since

Prajna Lindgren 8/26/15 2:09 PM

Deleted: was solely performed

Prajna Lindgren 9/23/15 11:11 PM

Deleted: derived from

Prajna Lindgren 8/24/15 3:20 PM

Deleted: , the classification results from MLC were further investigated to check the classification type and size of the seep mapped within a bubble patch. Based on bubble morphology described by Walter Anthony et al. (2010) and our field observations, we further refined

Prajna Lindgren 8/26/15 2:54 PM

Deleted: our classification results by integrating size as an additional feature to more accurately assign bubble patches with a seep type. Similar to training sample collection, for accuracy assessment, field-collected seep location data served as our ground truth.

Prajna Lindgren 8/31/15 10:10 AM

Deleted: further

Prajna Lindgren 8/31/15 10:11 AM

Deleted: We f

Prajna Lindgren 9/4/15 12:06 PM

Deleted: inally

1 location and year information, which served as marked point dataset for the model, to derive
2 and test the spatial characteristics of bubble patch distribution against a null hypothesis based
3 on complete spatial randomness. The null hypothesis suggests that the bubble patches are the
4 results of a spatially random process over the study area and thus the difference of spatial
5 pattern between years is random, i.e. the locations of bubble patches are independent when
6 comparing between years (Bivand et al., 2008). For this, we generated a multi-type nearest
7 neighbor distance function derived from the locations of the bubbles mapped in the images
8 using *Gcross* from the spatstat statistical package in R (Baddeley and Turner, 2005). *Gcross*
9 first determines clustering parameters for the dataset in the first year. These clustering
10 parameters are then used to model the expected number of the second year point given a
11 certain distance from the first year points if the second year point placement is random
12 relative the first year point placement. Based on the deviation between observed empirical
13 value and expected theoretical value estimated by the model, we determined the stability of
14 seep locations between 2011 and 2012. Similarly, we performed the multi-type nearest
15 neighbor distance function analysis using *Gcross* on the field dataset of Hotspot locations
16 collected in year 2011 and 2012 to check regularity of Hotspots.

17 We also considered that the centroid of a bubble patch, representing an ebullition bubble
18 patch point location, could move from one year to another due to changes in the shape and
19 size of a bubble patch or changes in bubble tube configuration in the sediment. We compared
20 the overlap area between ebullition patches mapped in 2011 and 2012 images. If some area of
21 a 2011 bubble patch appeared within the area of a 2012 bubble patch or vice versa, then we
22 considered bubble patch to be stable in location (i.e. reappearing). We assumed that the
23 overlapping bubble patches originated from the same point source seep. We checked location
24 stability among four classes of overlapping patches that were defined by setting thresholds on
25 area overlap; 'All overlapping bubble patches', 'More than 25% area overlap', 'More than
26 50% area overlap', 'More than 75% area overlap'.

27 We used a map of open-hole Hotspot seeps derived from UAV images to compare the
28 frequency of Hotspots with Hotspot occurrences observed during multiple years of fieldwork
29 by Greene et al. 2014.

30

Prajna Lindgren 9/6/15 9:52 PM
Deleted: C
Prajna Lindgren 9/6/15 9:52 PM
Deleted: S
Prajna Lindgren 9/6/15 9:52 PM
Deleted: R
Prajna Lindgren 9/6/15 9:53 PM
Deleted: (CSR)
Prajna Lindgren 9/6/15 9:52 PM
Deleted: CSR
Prajna Lindgren 9/24/15 10:41 AM
Deleted: events
Prajna Lindgren 9/24/15 10:41 AM
Deleted: created by a random process
Prajna Lindgren 9/24/15 10:43 AM
Deleted: h
Prajna Lindgren 9/24/15 10:43 AM
Deleted: are
Prajna Lindgren 9/24/15 10:44 AM
Deleted: from each other
Prajna Lindgren 9/24/15 10:45 AM
Deleted:
Prajna Lindgren 9/24/15 10:51 AM
Deleted: M
Prajna Lindgren 9/24/15 10:51 AM
Deleted: N
Prajna Lindgren 9/24/15 10:51 AM
Deleted: N
Prajna Lindgren 9/24/15 10:51 AM
Deleted: D
Prajna Lindgren 9/24/15 10:52 AM
Deleted: F
Prajna Lindgren 9/24/15 1:49 PM
Deleted: Thus, the <i>Gcross</i> function allowed us to describe seep clustering on the lake and compare that with the theoretical value generated based on the assumption that seep locations are completely random.
Prajna Lindgren 9/24/15 11:00 AM
Deleted: M
Prajna Lindgren 9/24/15 11:00 AM
Deleted: N
Prajna Lindgren 9/24/15 11:00 AM
Deleted: N
Prajna Lindgren 9/24/15 11:00 AM
Deleted: D
Prajna Lindgren 9/24/15 11:00 AM
Deleted: F
Prajna Lindgren 9/23/15 3:18 PM
Deleted: ice-free
Prajna Lindgren 9/19/15 11:07 PM
Deleted: s

4 Results and discussion

4.1 Relationship between bubble patch brightness and field-measured methane flux

We found that PC 1 brightness values of bubble patches correlated with the strength of field measured with the strength of field-measured methane flux of ebullition seeps (A, B, C and Hotspot seeps). The lowest mean PC 1 brightness belonged to A-type seep followed by B-type seep in both 2011 and 2012 (Figure 3). The highest mean PC 1 brightness was demonstrated by Hotspot in 2011 but C-type seep had slightly higher mean brightness in 2012 (Figure 3). Our ANOVA test rejected the null hypothesis that the mean PC 1 values of the different seep types are the same suggesting significant distinctions between mean PC 1 brightness values of different seep classes. Further post-hoc analysis using Tukey's HSD test demonstrated that C- and A-type, Hotspot and A-type, Hotspot and B-type seeps are significantly distinct based on their mean PC 1 with p-values < 0.05 (Supplement Table S2). We thus conclude that higher flux seeps (Hotspot and C-type) are associated with brighter bubble patches and lower flux seeps (A- and B type) are associated with darker bubble patches.

An absolute discrimination of individual seep type based on brightness was not supported by the post-hoc tests due to overlapping brightness ranges between different seep types (Fig. 3). This is likely because ebullition is episodic with varying bubbling rates over time and because individual low-flux methane seeps were not resolved given the spatial resolution of the image. A possible explanation for low PC 1 brightness of some Hotspots is that fresh thin night-time ice temporarily covered some Hotspots on the image acquisition day, allowing the formation of few small white gas bubbles while much of the remaining gas escaped through cracks in the thin ice, resulting in low true brightness for these high-flux seeps. We have observed this phenomenon on several occasions during our field visits in early winter and spring particularly on days when temperatures stayed low and Hotspots were covered with a few millimeters of ice with small bubbles beneath (Fig. 4); these Hotspots usually open up when atmospheric temperature rises again during the day. Conversely, Hotspots that remained open could not be identified in our snow-free lake ice imagery due to spectral similarities between open water and clear black ice (Fig. 1). ANOVA analysis was only performed on ice-covered Hotspots.

Prajna Lindgren 9/4/15 1:30 PM
Deleted: Characteristics of bubble patches in early winter lake ice imagery

Prajna Lindgren 9/4/15 1:31 PM
Deleted: Relationship between bubble patch brightness and field-measured methane ... [5]

Prajna Lindgren 11/11/15 12:21 PM
Formatted: Font:11 pt

Prajna Lindgren 9/8/15 8:50 PM
Deleted: grey

Prajna Lindgren 9/24/15 11:58 AM
Deleted: types

Prajna Lindgren 9/10/15 9:10 PM
Deleted:

Prajna Lindgren 8/31/15 11:13 AM
Deleted: with p-values < 0.05

Prajna Lindgren 9/10/15 9:25 AM
Deleted: at a 95% confidence interval

Prajna Lindgren 9/9/15 11:55 PM
Deleted: S

Prajna Lindgren 9/9/15 11:55 PM
Deleted: I

Prajna Lindgren 9/19/15 11:08 PM
Deleted: ,

Prajna Lindgren 9/19/15 11:08 PM
Deleted: ,

Prajna Lindgren 8/31/15 11:01 AM
Deleted: brighter bubble patches (low PC 1 values

Prajna Lindgren 8/31/15 11:01 AM
Deleted:)

Prajna Lindgren 9/19/15 11:08 PM
Deleted: types A

Prajna Lindgren 8/31/15 11:01 AM
Deleted: less bright bubble patches (high PC 1 values

Prajna Lindgren 8/31/15 11:02 AM
Deleted:)

Prajna Lindgren 9/10/15 9:28 PM
Deleted: was difficult to achieve

Prajna Lindgren 9/10/15 11:37 PM
Deleted:

Prajna Lindgren 9/8/15 9:03 PM
Deleted: low true brightness (high PC 1 values)

Prajna Lindgren 9/23/15 3:18 PM
Deleted: ice-free

1 We found that a large number of A-type seeps clustered together were not mapped as
2 individual bubble patches but rather as a single large bubble patch. A-type seeps and high flux
3 seeps that were close together were also mapped in a single feature associated with a brighter
4 bubble patch. Therefore, some A-type seeps showed low PC-1 brightness values. Similar to
5 A-type seeps, occasionally individual B-type seeps were also not distinct. In a time series
6 analysis of bubbling frequency by A- and B-type seeps, Walter Anthony et al. (2010) showed
7 that bubbling from these shallow-sourced seeps is highly seasonal. Bubbling rates are high in
8 summer when surface sediments are warmer, and low in winter when sediments cool down.
9 Bubble traps left in place over these seep types year-round revealed that low-flux seeps can
10 have periods of no bubbling for up to several months. Ice blocks harvested by us in spring
11 over seeps marked as A-type seeps in October confirm this pattern (Supplement Fig. S3). It is
12 very likely that A- and B-type seep conduits were present in the sediments, but not actively
13 bubbling during the two- and four-day periods after ice formation captured by the 2011 and
14 2012 imagery. Thus they did not appear under the given spatial resolution of the image and its
15 specific acquisition time. Also, bubble traps placed over C-type seeps year round revealed
16 that these seeps can also undergo long periods (weeks to months) of no bubbling, but when
17 they bubble, the bubbling rates are usually very high (Walter Anthony et al., 2010). This
18 intermittent flux behavior probably contributed to some discrepancies in the relationship
19 between bubble patch brightness derived from images that captured a snapshot of ebullition
20 activity and methane flux values of seeps estimated from long-term field observations (Table
21 1).

22 In other parts of Goldstream L., especially along the eastern shore, we found large patches of
23 ebullition bubbles (typically 3 to 10mm diameter) that formed large diffuse patches rather
24 than clustering as tightly packed bubbles the way A, B, C and Hotspot seeps do. In our optical
25 images, these ebullition bubbles appeared as irregular patches of fuzzy, white-colored bright
26 ice with some bright regular bubble spots (Fig. 4). Therefore, the brightness values
27 corresponding to the surrounding diffuse patches were assigned to other seeps, particularly to
28 low flux seeps that were within the patch and had not expressed completely when the images
29 were acquired. Until recently, these mm-scale ebullition bubbles were only recorded in
30 transect survey data as Tiny-type seep but never assigned a mean daily flux value or included
31 in whole-lake ebullition estimates due to a lack of associated flux data. Recent flux
32 measurements made continuously year-round with submerged bubble traps on the Tiny-type
33 seep class in Goldstream L. and other lakes suggest that flux from these seeps may also be

Prajna Lindgren 9/8/15 9:04 PM

Deleted: with low PC 1 values

Prajna Lindgren 9/8/15 9:04 PM

Deleted: (high true brightness)

Prajna Lindgren 9/24/15 12:03 PM

Deleted: difficult to map

Prajna Lindgren 9/9/15 11:56 PM

Deleted: II

important (Walter Anthony et al., unpublished). Analysis of bubbles collected with bubble traps placed over Tiny-type seeps revealed that these bubbles were 60–80% methane by volume (Walter Anthony et al., unpublished). When we extracted an ice block in spring 2013, we observed that Tiny-type ebullition had been frequent throughout winter, resulting in long, vertically oriented stacks of tiny ebullition bubbles trapped in ice (Fig. 4).

4.2 Classification of bubble patches

The overall MLC classification accuracy for differentiating seep types was ~ 50% for both 2011 and 2012 (Supplement Table S3). The classifier performed better to identify the lowest flux seeps (A-type) and the highest flux seeps (Hotspot-type). B-type and C-type seeps showed high error of commission mostly arising from the misidentification of seep A-type and Hotspots. C-type seeps had the largest error of omission since they were mostly misclassified as B-type seeps in 2011 and Hotspots in 2012.

Generally higher densities of A-type seeps (and also slightly in B- and C-type seeps) in ground surveys (Walter Anthony and Anthony, 2013; Greene et al., 2014) compared to aerial images (Table 1) can be explained by the time in which observations were made and image resolution. Results reported in Walter Anthony and Anthony (2013) and Greene et al. (2014) are based on ground surveys conducted over multiple years (2007-2011) at Goldstream L. usually one to two weeks following freeze-up when ice was safe to walk on (Walter Anthony et al., 2010). Since our aerial surveys were conducted only 2-4 days after ice formation, and the frequency of bubbling events from A-type seeps is often weeks to months in winter, it is not surprising that the field surveys several weeks after ice formation capture an order of magnitude more A-type seep bubbles. Additionally, it is very likely that some active A-type seeps that occurred in very small patches were not distinct under the given resolution of the aerial images. Relatively more frequent bubbling in B- and C-type seeps allows for similar seep density values between ground surveys and aerial images; however, as expected, the 2012 seep densities are closer to the ground-ice survey values due to (a) more time since freeze-up and (b) a much higher barometric pressure drop preceding the aerial image acquisition in October 2012 compared to October 2011. It is well established that ebullition dynamics are related to changes in barometric pressure (Mattson and Likens, 1990; Fechner-Levy and Hemond, 1996; Scandella et al., 2011).

Prajna Lindgren 9/4/15 1:38 PM

Deleted: In other parts of Goldstream L., especially along the eastern shore, we found large patches of Tiny-type seeps. When we extracted an ice block in spring 2013, we observed that Tiny-type ebullition had been frequent throughout winter, resulting in long, vertically oriented stacks of tiny ebullition bubbles trapped in ice (Fig. 4). In our optical images, tiny-type ebullition appeared as irregular patches of fuzzy, white-colored bright ice with some bright regular bubble spots (Fig. 4). Therefore, the brightness values corresponding to the surrounding Tiny-type seeps were assigned to other seeps, particularly to low flux seeps that were within the Tiny-seep patch and had not expressed completely when the images were acquired.

Prajna Lindgren 9/4/15 1:37 PM

Deleted: and estimation of whole-lake methane flux

Prajna Lindgren 9/4/15 1:32 PM

Deleted: with better performance in the 2012 image with 55% accuracy

Prajna Lindgren 9/19/15 11:52 PM

Deleted: is

Prajna Lindgren 11/7/15 7:35 AM

Deleted: inversely

The comparison of Hotspot densities in optical images vs. ground surveys in Table 1 also shows the expected pattern. The ground-survey data of Hotspots reflects multiple years of whole-lake Hotspots surveys when ice is thick enough to safely walk on. When ice is very thin a few days after freeze up more open holes are present on the lake and classified as Hotspot seeps in aerial images. A week or more later many holes freeze over and will be classified as C-type seeps in ground surveys. This could have also led to a high classification error for C-type seeps. The total density of C-type and Hotspot seeps combined remain consistent (~ 0.04 seeps m^{-2}) in both aerial and ground observations (Table 1). This also indicates that some of the seeps identified as Hotspots several days after freeze-up in aerial photos really become what we classify as C-type seeps (ice-sealed at the surface) within a week or more following freeze up.

4.3 Estimation of whole-lake methane flux

Our image-based analysis shows the whole-lake flux to be 174 ± 28 ml gas $\text{m}^{-2} \text{d}^{-1}$ and 216 ± 33 ml gas $\text{m}^{-2} \text{d}^{-1}$ for the year 2011 and 2012, respectively. The uncertainty terms are based on the standard error of the means of field-measured fluxes for seep classes. The higher flux estimate in 2012 is due to the presence of a larger number of bubble patches in 2012 (0.185 seeps m^{-2}) compared to 2011 (0.119 seeps m^{-2}) (Table 1). The field-based estimate of whole-lake ebullition for Goldstream L. using ice-bubble transect surveys (170 ± 54 ml gas $\text{m}^{-2} \text{d}^{-1}$), was slightly at the low end of the estimates based on optical imagery analysis from 2011 and 2012 respectively. It is conceivable that the field-based transect surveys might yield a lower flux than whole-lake seep analyses given that seeps are spatially rare, and field surveys often cover $<1\%$ of the lake surface area (Walter Anthony and Anthony, 2013). However, on Goldstream L., where our field transect bubble surveys covered 13% of the lake area for A, B and C-type seeps and 100% of the lake area for Hotspots, the higher estimates based on optical imagery appear to be due to an overestimation of Hotspots in the early-acquisition date aerial image analysis. It is important to note that while the whole-lake methane flux estimates from our aerial survey are close to those based on ground surveys, the flux estimates for individual seep types may vary between the methods. It is also possible that with aerial surveys we are underestimating the total contribution of methane flux from low flux seeps because they had not expressed completely when we acquired our aerial photos and that we are overestimating the contribution from high flux seeps.

Prajna Lindgren 9/9/15 6:45 PM

Deleted: We used the classification results to estimate seep density and a whole-lake ebullition rate.

4.4 Spatial distribution of bubble patches in relation to thermokarst-lake margin

High methane production in response to thermokarst activity on the Goldstream L. is evident from the distribution pattern of ebullition bubble patches at the eroding margins in different years. We found a strong inverse relationship (R^2 values of 0.86 and 0.79 for the years 2011 and 2012, respectively, with p -values < 0.05) between ebullition bubble patch area covering the lake ice and distance from the rapidly eroding eastern margin of the lake (Fig. 5). The percent surface area of lake ice covered with ebullition bubble patches ice decreased with distance from the active erosion margin. Thermo-erosion as well as talik growth on the expanding eastern shore release labile Pleistocene-aged organic matter as permafrost thaws, enhancing anaerobic microbial activity in the lake and talik sediments, and leading to enhanced methane emissions along this shore (Brosius et al., 2012; Walter Anthony and Anthony, 2013). Holocene-aged carbon from vegetation and active layer soils is also eroded and additionally produced within the lake, further fueling microbial methane production (Walter Anthony et al., 2014). Walter Anthony and Anthony, 2013 found an interesting relationship between lake bed morphology and ebullition bubble seep density on Goldstream L.. They found dense cluster of ebullition seeps distributed ~ 10 m apart across the lake that matched the spacing of baydjarkah on the lake bed. This indicates that most of the methane gas bubbles originated from the top of baydjarkhs consisting of organic-rich thawed permafrost soil. While we did not conduct specific analyses in our study, such patterns should be detectable in optical remote sensing images of lake ice as well.

We observed fewer ebullition bubble patches in the center of the lake, which we interpret as a sign that labile Pleistocene-aged organic carbon in the talik under this area has been largely depleted, and unlike at the edge along the active erosion margin, there is no significant additional accumulation of ancient labile carbon in the lake center (Brosius et al., 2012). Radiocarbon dating of bubble patches found in the lake center showed that these seeps originate from Holocene-aged and more recent organic matter that is found in the upper lake sediments (Brosius et al., 2012). Generally, methane bubbling was the lowest along the 1949 eastern lake margin and the highest along the 2012 eastern lake margin (Fig. 5), indicating that depletion of labile carbon progressed since these areas were included in the lake and the active thermo-erosion margin migrated eastward. This shows that optical remote sensing is a powerful tool to understand the spatial variability of methane ebullition on thermokarst lakes.

Prajna Lindgren 9/4/15 1:34 PM

Deleted: <#>Spatial and temporal characteristics of bubble patches on early winter lake ice .

Prajna Lindgren 9/4/15 1:39 PM

Deleted: also

4.5 Multi-year comparison of bubble patch characteristics: 2011 and 2012

We observed four possible characteristics of bubble patch dynamics in our images (Fig. 6). (i) Bubble patches may move horizontally; (ii) Bubble patches do not maintain the same morphology between years (e.g. single bubble patches re-appear in a cluster of multiple patches the next year or vice-versa); (iii) Bubble patches appear in an image in one year and not another; and (iv) Bubble patches maintain the location and shape but patch size is different between the years. It is important to note that these observations are made during the two very short windows of time 2-4 days after freeze-up. Our analysis does not take into account the changes in long-term bubble patch morphology. Hence, it is important to highlight that the characteristics of bubble patches are driven by the dynamics of bubble formation and transport, hydrostatic pressure, and ice growth. Other changes in the characteristics of bubble patches could be because of evolution of point sources or changes in point source conduits (bubble tubes) in the sediment (Walter et al., 2008a; Scandella et al., 2011). Atmospheric pressure dynamics can also strongly impact bubbling over short time scales, resulting in different ice-bubble patterns one year from the next if insufficient time passes to allow all seeps to be expressed in the lake ice cover. Field measurements have shown that ebullition is related to changes in hydrostatic pressure (Mattson and Likens, 1990; Varadharajan, 2009; Casper et al., 2000; Glaser et al., 2004; Tokida et al., 2007; Scandella et al., 2011). A significant air pressure drop during the week preceding image acquisition in October 2012 may have allowed methane that previously accumulated in the sediment during high-pressure days to rise up into the water column, manifesting itself as larger numbers of bubbles (Fig. 7), and larger and brighter bubble-patches in the lake ice (Fig. 6). Conversely, air pressure change in October 2011 was not large enough to enhance ebullition before the image was acquired. As a result, bubble patch density was 55% higher in 2012 (0.185 m^{-2}) 2012 compared to 2011 (0.119 m^{-2}). Similarly, the estimated mean whole-lake ebullition was 24% higher in 2012 compared to 2011 due to different atmospheric pressure dynamics. However, the general spatial distribution of bubble patches remained the same between the two years: ebullition bubble patches were more concentrated towards the eastern thermokarst lake shore.

We rejected the null hypothesis of complete spatial randomness to show that the difference in spatial patterns of bubble patches and Hotspots between years is not random, i.e. that the locations of seeps in the years 2011 and 2012 are not independent. The *Gcross* distribution

Prajna Lindgren 9/4/15 1:40 PM

Deleted: a

Prajna Lindgren 9/4/15 1:40 PM

Deleted: b

Prajna Lindgren 11/7/15 7:54 AM

Deleted: n't

Prajna Lindgren 9/4/15 1:40 PM

Deleted: c

Prajna Lindgren 9/4/15 1:40 PM

Deleted: d

Prajna Lindgren 11/11/15 12:08 PM

Deleted: inversely

Prajna Lindgren 9/6/15 11:47 AM

Deleted: sizes

Prajna Lindgren 9/6/15 11:48 AM

Deleted: 7

Prajna Lindgren 9/24/15 11:52 AM

Deleted: The *Gcross* distribution functions for marked bubble patch locations derived from images and for Hotspot locations derived from DGPS field datasets agree on regularities of seep locations across time (Fig. 8). The deviation between the observed empirical value (black curve) and theoretical expected value assuming the points are completely random (red curve) in *Gcross* function, suggests that a large and statistically significant number of bubble patches and Hotspot seeps show spatial dependence between years 2011 and 2012 (Fig. 8). The empirical curves in both cases lie well above the gray shaded area, which is the 95% critical confidence band for theoretical assumption of complete spatial randomness and independence. The plot for

Prajna Lindgren 9/24/15 11:50 AM

Deleted: bubble patch

1 function showed that a statistically significant number of second year bubble patch center
2 points are less than 2 meters away from the first year center points and that there are far less
3 than expected that are 3 meters or more apart (Fig. 8a). For the Hotspots, a statistically
4 significant number of seeps moved less than a meter (Fig. 8b). Since, our image rectification
5 accounted for geolocation error of less than 20 cm and DGPS geolocation error is even
6 smaller and negligible, we conclude that the seep locations are consistent between years 2011
7 and 2012.

8 Based on our DGPS data, the number of Hotspots was relatively stable among the various
9 surveys with about 105 Hotspots for the whole lake as the average of various measurements
10 during different years and spring and fall field seasons (Greene et al., 2014). UAV-based
11 aerial images taken five days after ice formation when snow covered the lake also
12 demonstrated close agreement with the Hotspot seep numbers and locations. We were able to
13 identify 78 dark open-water holes in the white, snow-covered UAV lake image acquired in
14 early winter of 2012. Among these 78 locations there was a total of about ~ 95-100 active
15 open-hole Hotspot seeps since some large, irregularly shaped holes consisted of multiple,
16 coalesced holes produced by Hotspot seeps of close proximity (Supplement Fig. S4).

17 When we compared the location of bubble patches in 2011 and 2012, we found that 47.2% of
18 total 1195 ebullition bubble patches mapped in 2011 reappeared in 2012, which is 35.7% of
19 total 1860 ebullition bubble patches mapped in 2012. We found that 37.5%, 30% and 17.7%
20 of bubble patches mapped in 2011 reappeared in 2012 with an overlap area of 'more than
21 25%', 'more than 50%' and 'more than 75% area', respectively. We expect that if more time
22 passed between the time of freeze-up and aerial image acquisition date we would see an even
23 higher percentage of seep location re-occurrences because more seeps would be actively
24 expressed.

25 We also observed a relationship between bubble patch brightness and location stability of
26 bubble patches. Very bright patches in 2012 seemed to appear at locations where bubble
27 patches were already observed in 2011. This could indicate locations of high flux seeps where
28 methane was able to rise through the sediment even under relatively high hydrostatic pressure
29 conditions that we observed in October 2011. Based on our bubble patch classification results
30 (Table 1), we also noticed that seep density of high-flux C- and Hotspot-type seeps is less
31 variable during our study period compared to low-flux A- and B-type seeps. However, long-
32 term remote sensing and ground-based observations are required to further test our hypothesis

Prajna Lindgren 9/6/15 12:34 PM

Deleted: s

Prajna Lindgren 9/6/15 12:34 PM

Deleted: The observed function for the DGPS Hotspot locations rises almost vertically over separation distances of 0-1 meter deviating away from the theoretical function.

Prajna Lindgren 9/10/15 10:08 AM

Deleted: Therefore

Prajna Lindgren 9/10/15 10:10 AM

Deleted:

Prajna Lindgren 9/23/15 3:18 PM

Deleted: ice-free

Prajna Lindgren 9/9/15 11:58 PM

Deleted: III

Prajna Lindgren 9/19/15 11:39 PM

Deleted: (Table 2)

Prajna Lindgren 9/6/15 12:01 PM

Deleted: Using thresholds of area overlap in our evaluation of seep location stability w

Prajna Lindgren 9/6/15 12:02 PM

Deleted: when we considered bubble patches

Prajna Lindgren 9/6/15 12:03 PM

Deleted: area overlap

Prajna Lindgren 9/6/15 12:03 PM

Deleted: overlap

Prajna Lindgren 9/6/15 12:04 PM

Deleted: overlap

Prajna Lindgren 9/10/15 9:59 PM

Deleted: Increased brightness in 2012 of re-occurring ebullition bubble patches

Prajna Lindgren 9/19/15 11:15 PM

Deleted: in

1 of seep regularity that high flux seeps are temporally more stable in their location than low
2 flux seeps. Additionally, long-term data may also help to account for the difference in
3 pressure and look at possible changes in seep type over the years.

4 The regularity of bubble patches observed despite the differences in atmospheric pressure
5 conditions following the lake freeze-up events in 2011 and 2012 as well as the location
6 stability of Hotspots indicates that a large number of point source seeps in thermokarst lakes
7 are stable over at least annual time-scales. Walter Anthony et al. (2010) also found seeps to
8 maintain stable locations in Goldstream L. when submerged bubble traps were placed over
9 individual seeps to monitor their ebullition dynamics for periods of up to 700 days. In Siberia
10 one Hotspot seep location was marked and found stable for at least eight years (Walter
11 Anthony et al., 2010).

13 5 Benefits and challenges of aerial image analysis for ebullition seep 14 mapping

15 We found numerous significant benefits of using aerial images for characterizing ebullition
16 seeps on lake ice. Aerial images of early winter lake ice without snow cover allowed us to
17 map and characterize bubble patches on the entire lake surface as well as assess their spatial
18 distribution more accurately. While snow-covered lake ice image allowed us to map open-
19 hole Hotspots. We were able to differentiate high methane emitting seeps from low methane
20 emitting seeps on the lake based on PC 1 brightness values of bubble patches. Image-derived
21 estimates of seep densities by class agreed with those of field-based survey methods, except
22 for some overestimation of Hotspots and underestimation of A-type seeps. We were able to
23 differentiate lake areas with high seep densities versus low seep densities; having this ability
24 is especially useful for quantifying methane ebullition on larger lakes that are harder to survey
25 extensively by foot.

26 Our results also imply a potential to apply high-resolution optical images at a regional scale to
27 quantify relative methane flux from many lakes, which at a minimum should allow for
28 classification of high-ebullition versus low-ebullition lakes and their distribution in a region.
29 It is important to note, that while image analysis is useful to comprehensive mapping of lake-
30 ice bubbles, for the estimation of whole-lake methane emissions this technique should be
31 coupled with bubble-trap field measurements of bubble collection using bubble traps and
32 laboratory measurements of methane concentration in bubbles.

Prajna Lindgren 9/5/15 10:38 PM

Deleted:

Prajna Lindgren 9/4/15 1:55 PM

Deleted: Our results show that ebullition bubble patches can be mapped to high precision in aerial imagery.

Prajna Lindgren 9/4/15 1:56 PM

Moved (insertion) [3]

Prajna Lindgren 9/20/15 12:09 AM

Deleted:

Prajna Lindgren 9/19/15 11:20 PM

Deleted: other

Prajna Lindgren 9/19/15 11:20 PM

Deleted: ,

1 But because ebullition is a temporally dynamic phenomenon, our ability to accurately identify
2 the distinct seep type of bubble patches on a snapshot of ebullition activity during only 2- and
3 4-days since lake ice formation is limited. The morphology and distribution of bubbles can
4 undergo significant changes in response to freeze/thaw cycles during winter (Jeffries et al.,
5 2005). Furthermore, ebullition is highly controlled by the balance between atmospheric
6 pressure and sediment strength making it an episodic phenomenon (Varadharajan, 2009;
7 Scandella et al., 2011). Ebullition is triggered following the falling of hydrostatic pressure or
8 after a sufficient volume of gas is produced in the sediment that allows “bubble-tubes” or “gas
9 conduits” in lake sediments to open or dilate (Scandella et al., 2011). Bubbles previously
10 trapped in lake sediment then break out through these open “bubble-tubes” and rise up in the
11 water column. Moreover, microbial activity of methane producing bacteria is temperature
12 dependent. As a result, seep ebullition slows down when the lake surface sediments cool
13 down in winter and it increases as lake sediment warms up in summer (Walter Anthony and
14 Anthony, 2010). Therefore, discrepancies arise in estimates of the number of seeps and seep
15 morphology derived from observations made at different times of the ice cover season (Wik et
16 al., 2011). Ideally, optical image acquisition would occur at least several weeks following
17 freeze-up of lakes to allow more time for seep expression in lake ice. Unfortunately, snow-
18 free conditions several weeks after freeze-up is rare in many regions of the Arctic and early
19 snow cover inhibits the mapping of bubble patches with optical data.

20 SAR data has an advantage over optical remote sensing data in detecting methane bubbles
21 trapped in lake ice under snow cover conditions (Walter et al. 2008; Engram et al., 2012).
22 Engram et al., 2012 showed that particularly L-band SAR data acquired in the fall has the
23 potential to estimate whole lake methane ebullition since longer wave length L-band is able to
24 detect bubbles under other conditions such as presence of snow, thin layer of white ice, and
25 aquatic vegetation. However, the moderate spatial resolution of current L-band SAR systems
26 can be a limiting factor to estimate methane emission from small lakes and to capture delicate
27 spatial patterns of ebullition seeps on lakes. SAR lake images further tend to have false
28 backscatter signals from the lake shore (Walter et al. 2008; Engram et al., 2012), therefore
29 limiting its usability in proximity to shores (about 1 pixel around lake shores is excluded in
30 SAR analyses) where we show an important component of ebullition may take place on
31 eroding thermokarst margins. Thus, high-resolution optical images can supplement SAR-
32 based studies by revealing the location of methane ebullition seeps and their types on the lake
33 more precisely. Our study shows that optical high-resolution remote sensing methods have the

Prajna Lindgren 9/4/15 1:57 PM

Deleted:

Prajna Lindgren 8/31/15 9:38 PM

Deleted:

potential, given the caveats raised above, to improve understanding of spatial and temporal variability of ebullition and therefore the dynamics of microbial processing of organic matter within an individual lake.

6 Conclusions

It is important to understand the dynamics of methane ebullition from thermokarst lakes to estimate the amount of carbon release from thawing permafrost and evaluate its feedback to the global carbon cycle. Our study focusing on Goldstream L., Interior Alaska, shows that high-resolution optical remote sensing is a promising tool to map the distribution of point source methane ebullition seeps across an entire thermokarst lake surface, a task that is difficult to achieve through field-based surveys alone. This method helps to reveal the location and relative sizes of high- and low-flux seepage zones within lakes. We also demonstrated that a large proportion of ebullition seeps in the study lake were location stable over at least two winter seasons in the 2011-2012 observation period. Such observations may be used to indirectly characterize permafrost carbon mobilization in a lake since lake portions with greater numbers of high flux seeps likely either the presence of rapidly thawing organic-rich permafrost deposits or eroding lake margins. Our approach is also applicable to other regions and will help to characterize methane ebullition emissions from seasonally ice-covered lakes, including thermokarst and non-thermokarst lakes in tundra and boreal zones. It will help to differentiate lakes in a region based on methane emission by estimating ebullition seep density, and their relative methane flux. This differentiation could potentially be used to identify presence or absence of organic-rich permafrost deposits such as yedoma in the area. For example yedoma-type thermokarst lakes such as Goldstream L., where large amounts of labile carbon is readily available for microbes to decompose, emit more methane than non-yedoma-type thermokarst lakes. This can be a useful supplement to surveying soil carbon pools and yedoma distribution at a regional scale. Multi-temporal spatial information derived from remotely sensed optical data allows identification of variables that control methane ebullition dynamics and spatial patterns. However, the timing of optical image acquisitions is a critical and a potentially limiting factor, with respect to both atmospheric pressure changes and snow/no-snow conditions during early lake freeze up. Therefore, high-resolution remotely sensed optical images in combination with SAR and field data could be a very valuable tool to improve the estimation of methane emission from lakes at the regional scale.

Prajna Lindgren 8/31/15 10:45 PM

Deleted: Despite these challenges, we found numerous significant benefits of using aerial images for characterizing ebullition seeps on lake ice. Aerial images of early winter lake ice without snow cover allow to map and characterize bubble patches on the entire lake surface as well as assess their spatial distribution more accurately. We were able to differentiate high methane emitting seeps from low methane emitting seeps on the lake based on bubble patch brightness. Image-derived estimates of seep densities by class agreed with those of field-based survey methods, except for the understandable problems of overestimating Hostspots and underestimating A-type seeps. We were able to differentiate lake areas with high seep densities versus low seep densities; this ability could be especially important on larger lakes that are h... [6]

Prajna Lindgren 9/4/15 1:56 PM

Moved up [3]: Our results also imply a potential to apply high resolution optical images at a re... [7]

Prajna Lindgren 9/4/15 4:30 PM

Deleted: ... [8]

Prajna Lindgren 8/31/15 1:01 PM

Deleted: ... [9]

Prajna Lindgren 8/31/15 11:00 PM

Deleted: ing

Prajna Lindgren 8/31/15 11:05 PM

Moved down [1]: However, the timing of image acquisition is a critical and potentially limiti... [11]

Prajna Lindgren 8/31/15 1:03 PM

Moved (insertion) [2]

Prajna Lindgren 8/31/15 3:10 PM

Deleted: Such observations may also be used to indirectly characterize permafrost carbon... [10]

Prajna Lindgren 11/11/15 11:29 AM

Deleted: Our approach

Prajna Lindgren 11/11/15 11:29 AM

Formatted: Font:Not Bold

Prajna Lindgren 9/19/15 11:25 PM

Deleted: is applicable to

Prajna Lindgren 9/19/15 11:25 PM

Deleted: other regions and will help to

Prajna Lindgren 8/31/15 3:14 PM

Deleted: characterize

Prajna Lindgren 8/31/15 1:05 PM

Deleted: methane ebullition emissions from seasonally ice-covered lakes, including then... [12]

Prajna Lindgren 8/31/15 11:05 PM

Moved (insertion) [1]

Prajna Lindgren 8/31/15 3:16 PM

Deleted: R

Prajna Lindgren 8/31/15 3:16 PM

Deleted: , multi-temporal spatial information allows identification of variables that contro... [13]

Prajna Lindgren 8/31/15 1:03 PM

Moved up [2]: Such observations may also be used to indirectly characterize permafrost ca... [14]

Prajna Lindgren 9/10/15 11:42 PM

Deleted: ...

1 **Acknowledgements**

2 We thank A. Bondurant for harvesting ice blocks; P. Anthony for statistical coding; and A.
3 Strohm, M. Engram and J. Lenz for assistance with other field work. We thank J. Cherry for
4 aerial image acquisitions and B. Crevensten and G. Walker for UAV image acquisitions. This
5 research was funded by NASA Carbon Cycle Science grant #NNX11AH20G. Additional
6 support came from NSF # 1107892.

8 **Author contributions**

9 G. Grosse and K. M. Walter Anthony conceived this study. P. R. Lindgren developed the
10 method, performed data analysis, and wrote the manuscript with significant input from all co-
11 authors. P. R. Lindgren, G. Grosse and K. M. Walter Anthony were responsible for the field
12 work.

14 **References**

- 15 Baatz, M. and Schäpe, A.: Multiresolution segmentation - an optimization approach for high
16 quality multi-scale image segmentation. *Angewandte Geographische*
17 *Informationsverarbeitung XII, Beiträge zum AGIT-Symposium Salzburg 2000*, 12-23.
18 Herbert Wichmann Verlag, Karlsruhe, 2000.
- 19 Baddeley, A. and Turner, R.: Spatstat: An R package for analyzing spatial point patterns, *J.*
20 *Stat. Software*, 12(6), 1–42, URL: www.jstatsoft.org, ISSN: 1548–7660, 2005.
- 21 Bastviken, D.: Methane emissions from lakes: Dependence of lake characteristics, two
22 regional assessments, and a global estimate, *Global Biogeochem. Cycles*, 18(4), 1–12,
23 doi:10.1029/2004GB002238, 2004.
- 24 Bastviken, D., Tranvik, L. J., Downing, J. A., Crill, P. M., and Enrich-Prast, A.: Freshwater
25 methane emissions offset the continental carbon sink, *Science*, 331, 50,
26 doi:10.1126/science.1196808, 2011.
- 27 Bivand, R. S., Pebesma, E. J., and Gomez-Rubio, V.: *Applied Spatial Data Analysis with R*,
28 Springer, New York, 2008.

- 1 Blaschke, T. and Strobl, J.: What's wrong with pixels? Some recent developments interfacing
2 remote sensing and GIS, *GIS – Zeitschrift für Geoinformationssysteme*, 14 (6), 12–17, 2001.
- 3 Blaschke, T., Lang, S., and Hay, G. J.: *Object Based Image Analysis: Spatial Concepts for*
4 *Knowledge-Driven Remote Sensing Applications*, Springer-Verlag Berlin Heidelberg,
5 Germany, 2008.
- 6 Boereboom, T., Depoorter, M., Coppens, S., and Tison, J.-L.: Gas properties of winter lake
7 ice in Northern Sweden: implication for carbon gas release, *Biogeosciences*, 9(2), 827–838.
8 doi:10.5194/bg-9-827-2012, 2012.
- 9 Brosius, L. S., Walter Anthony, K. M., Grosse, G., Chanton, J. P., Farquharson, L. M.,
10 Overduin, P. P., and Meyer, H.: Using the deuterium isotope composition of permafrost
11 meltwater to constrain thermokarst lake contributions to atmospheric CH₄ during the last
12 deglaciation, *J. Geophys. Res.*, 117(G1), G01022, doi:10.1029/2011JG001810, 2012.
- 13 Canny, J.: A computational approach to edge detection, *IEEE Trans. Pattern Analysis &*
14 *Machine Intelligence*, 8, 679-714, 1986.
- 15 Casper, P., Maberly, S. C., Hall, G. H., and Finlay, B. J.: Fluxes of methane and carbon
16 dioxide from a small productive lake to the atmosphere, *Biogeochemistry*, 49, 1–19, 2000.
- 17 Definiens, *Segmentation Algorithms In Definiens Developer 7 Reference Book*, Document
18 Version 7.0.0.843, 15-27, Definiens AG, München, Germany, 2007a.
- 19 Definiens, *Edge Extraction Canny In Definiens Developer 7 Reference Book*, Document
20 Version 7.0.0.843, 62-63, Definiens AG, München, Germany, 2007b.
- 21 Duguay, C. R. and Lafleur, P. M.: Determining depth and ice thickness of shallow sub-Arctic
22 lakes using space-borne optical and SAR data, *Int. J. Remote Sens.*, 24(3), 475–489,
23 doi:10.1080/01431160304992, 2003.
- 24 Engram, M., Walter Anthony, K., Meyer, F. J., and Grosse, G.: Characterization of L-band
25 synthetic aperture radar (SAR) backscatter from floating and grounded thermokarst lake ice in
26 Arctic Alaska, *Cryosph.*, 7(6), 1741–1752, doi:10.5194/tc-7-1741-2013, 2013.
- 27 Engram, M., Walter Anthony, K. M., Meyer, F. J., and Grosse, G.: Synthetic aperture radar
28 (SAR) backscatter response from methane ebullition bubbles trapped by thermokarst lake ice,
29 *Canadian Journal of Remote Sensing*, 38(6), 667–682, 2012.

1 Estornell, J., Marti-Gavila, J. M., Teresa Sebastia, M., and Mengua, J.: Principal component
2 analysis applied to remote sensing, *Modelling in Science Education and Learning*, 6(2), 83-
3 89, 2013.

4 Fechner-Levy, E. J. and Hemond, H. F.: Trapped methane volume and potential effects on
5 methane ebullition in a northern peatland, *Limnol. Oceanogr.*, 41(7), 1375–1383, 1996.

6 Glaser, P. H., Chanton, J. P., Morin, P., Rosenberry, D. O., Siegel, D. I., Ruud, O., Chasar, L.
7 I., and Reeve, A. S.: Surface deformations as indicators of deep ebullition fluxes in a large
8 northern peatland, *Global Biogeochem. Cycles*, 18, GB1003, doi:10.1029/2003GB002069,
9 2004.

10 Greene, S., Walter Anthony, K. M., Archer, D., Sepulveda-Jauregui, A., and Martinez-Cruz,
11 K.: Modeling the impediment of methane ebullition bubbles by seasonal lake ice,
12 *Biogeoscience Discuss.*, 11, 10863–10916, 2014. <http://doi:10.5194/bgd-11-10863-2014>.

13 Grosse, G., Harden, J., Turetsky, M., McGuire, A. D., Camill, P., Tarnocai, C., Frolking, S.,
14 Schuur, E. A. G., Jorgenson, T., Marchenko, S., Romanovsky, V., Wickland, K. P., French,
15 N., Waldrop, M., Bourgeau-Chavez, L., and Striegl, R. G.: Vulnerability of high-latitude soil
16 organic carbon in North America to disturbance, *J. Geophys. Res.*, 116, 1–23,
17 doi:10.1029/2010JG001507, 2011.

18 Grosse, G., Jones, B., and Arp, C.: Thermokarst Lakes, Drainage and Drained Basins,
19 *Treatise Geomorphol.*, 8, 325–353, 2013.

20 Hinzman, L.D., Bettez, N. D., Bolton, W. R., Chapin, F. S., Dyurgerov, M. B., Fastie, C. L.,
21 Griffith, B., Hollister, R. D., Hope, A., Huntington, H. P., Jensen, A. M., Jia, G. J., Jorgenson,
22 T., Kane, D. L., Klein, D. R., Kofinas, G., Lynch, A. H., Lloyd, A. H., McGuire, A. D.,
23 Nelson, F. E., Oechel, W. C., Osterkamp, T. E., Racine, C. H., Romanovsky, V. E., Stone, R.
24 S., Stow, D. A., Sturm, M., Tweedie, C. E., Vourlitis, G. L., Walker, M. D., Walker, D. A.,
25 Webber, P. J., Welker, J. M., and Winker, K. S.: Evidence and Implications of Recent Climate
26 Change in Northern Alaska and Other Arctic Regions, *Clim. Change*, 72(3), 251–298,
27 doi:10.1007/s10584-005-5352-2, 2005.

28 Hugelius, G. et al.: Improved estimates show large circumpolar stocks of permafrost carbon
29 while quantifying substantial uncertainty ranges and identifying remaining data gaps,
30 *Biogeosciences Discuss.*, 11(3), 4771–4822, doi:10.5194/bgd-11-4771-2014, 2014.

1 Jeffries, M. O., Morris, K., Weeks, W. F., and Wakabayashi, H.: Structural and stratigraphic
2 features and ERS 1 synthetic aperture radar backscatter characteristics of ice growing on
3 shallow lakes in NW Alaska, winter 1991-1992, *J. Geophys. Res.*, 99(C11), 22459–22471,
4 1994.

5 Jeffries, M. O., Morris, K., and Kozlenko, N.: Ice Characteristics and Remote Sensing of
6 Frozen Rivers and Lakes, *Remote Sensing in Northern Hydrology: Geophysical Monograph*
7 *Series*, 163, 63-90, 2005.

8 Jorgenson, M. T. and Shur, Y.: Evolution of lakes and basins in northern Alaska and
9 discussion of the thaw lake cycle, *J. Geophys. Res.*, 112(F2), 1–12,
10 doi:10.1029/2006JF000531, 2007.

11 Kanevskiy, M., Shur, Y., Fortier, D., Jorgenson, M. T., and Stephani, E.: Cryostratigraphy of
12 late Pleistocene syngenetic permafrost (yedoma) in northern Alaska, Itkillik River exposure,
13 *Quat. Res.*, 75(3), 584–596, doi:10.1016/j.yqres.2010.12.003, 2011.

14 Keller, M. and Stallard, R. F.: Methane emission by bubbling from Gatun Lake, Panama, *J.*
15 *Geophys. Res.*, 99, 8307–8319, doi:10.1029/92JD02170, 1994.

16 Kessler, M. A., Plug, L. J., and Walter Anthony, K. M.: Simulating the decadal- to millennial-
17 scale dynamics of morphology and sequestered carbon mobilization of two thermokarst lakes
18 in NW Alaska, *J. Geophys. Res. Biogeosciences*, 117(G2), 1-22, doi:10.1029/2011JG001796,
19 2012.

20 Kokelj, S. V. and Jorgenson, M. T.: Advances in Thermokarst Research, *Permafr. Periglac.*
21 *Process.*, 24(2), 108–119, doi:10.1002/ppp.1779, 2013.

22 Koven, C. D., Ringeval, B., Friedlingstein, P., Ciais, P., Cadule, P., Khvorostyanov, D.,
23 Krinner, G., and Tarnocai, C.: Permafrost carbon-climate feedbacks accelerate global
24 warming, *Proc. Natl. Acad. Sci.*, 108, 14769–14774, doi:10.1073/pnas.1103910108, 2011.

25 Langer, M., Westermann, S., Walter Anthony, K. M., Wischniewski, K., and Boike, J.: Frozen
26 ponds: production and storage of methane during the Arctic winter in a lowland tundra
27 landscape in northern Siberia, Lena River Delta, *Biogeosciences Discuss.*, 11(7), 11061–
28 11094, doi:10.5194/bgd-11-11061-2014, 2014.

29 Mather, P.: *Pattern Recognition Principles In Classification for Remotely Sensed Data*,
30 Second Edition, 41-75, CRC Press, New York, 2009.

1 Mattson, M. D. and Likens, G. E.: Air pressure and methane fluxes, *Nature*, 347, 718–719,
2 1990.

3 Navulur, K.: *Multispectral Image Analysis Using the Object-Oriented Paradigm*, CRC Press,
4 Boca Raton, FL, 2007.

5 Péwé, T. L.: Quaternary geology of Alaska, U.S. Geol. Survey Professional Paper 835, 1975.

6 Phelps, A. R., Peterson, K. M., and Jeffries, M. O.: Methane efflux from high-latitude lakes
7 during spring ice melt. *J. Geophys. Res. Atmos.* 103:29029-29036, doi:10.1029/98JD00044,
8 1998.

9 Plug, L. J. and West, J. J.: Thaw lake expansion in a two-dimensional coupled model of heat
10 transfer, thaw subsidence, and mass movement, *J. Geophys. Res.*, 114(F1), F01002,
11 doi:10.1029/2006JF000740, 2009.

12 Rowland, J. C., Travis, B. J., and Wilson, C. J.: The role of advective heat transport in talik
13 development beneath lakes and ponds in discontinuous permafrost, *Geophys. Res. Lett.*,
14 38(17), 1–5, doi:10.1029/2011GL048497, 2011.

15 Rocchini, D., Ricotta, C., and Chiarucci, A.: Using satellite imagery to assess plant species
16 richness: The role of multispectral systems systems, *Applied Vegetation Science*, 10, 325-
17 332, 2007.

18 Scandella, B. P., Varadharajan, C., Hemond, H. F., Ruppel, C., and Juanes, R.: A conduit
19 dilation model of methane venting from lake sediments, *Geophys. Res. Lett.*, 38(6), 1-6,
20 doi:10.1029/2011GL046768, 2011.

21 Schowengerdt, A.: *Principal Components In Remote sensing: Models and methods for image*
22 *processing*, Third Edition, 193-199, Academic Press, San Diego, CA, 2007.

23 Schuur, E. A. G., Bockenheim, J., Canadell, J. P., Euskirchen, E., Field, C. B., Goryachkin, S.
24 V., Hagemann, S., Kuhry, P., Lafleur, P. M., Lee, H., Mazhitova, G., Nelson, F. E., Rinke, A.,
25 Romanovsky, V. E., Shiklomanov, N., Tarnocai, C., Venevsky, S., Vogel, J. G. and Zimov, S.
26 A.: Vulnerability of Permafrost Carbon to Climate Change: Implications for the Global
27 Carbon Cycle, *Bioscience*, 58(8), 701, doi:10.1641/B580807, 2008.

28 Sepulveda-Jáuregui, A., Walter Anthony, K. M., Martinez-Cruz, K., Greene, S., and F.
29 Thalasso. Methane and carbon dioxide emissions from 40 lakes along a north-south latitudinal
30 transect in Alaska. *Biogeosciences Discuss.*, 11, 13251-13307, 2014.

1 Smith, L. C., Sheng, Y., and MacDonald, G. M.: A first pan-Arctic assessment of the
2 influence of glaciation, permafrost, topography and peatlands on northern hemisphere lake
3 distribution, *Permafrost and Periglacial Processes*, 18(2), 201-208, 2007.

4 Tokida, T., Miyazaki, T., and Mizoguchi, M.: Ebullition of methane from peat with falling
5 atmospheric pressure, *Geophys. Res. Lett.*, 32, L13823 10.1029/2005GL022949, 2005.

6 Varadharajan, C.: Magnitude and spatio-temporal variability of methane emissions from a
7 eutrophic freshwater lake, PhD thesis, Massachusetts Institute of Technology, Cambridge,
8 MA, 2009.

9 Walter, K. M., Zimov, S. A., Chanton, J. P., Verbyla, D., and Chapin, F. S.: Methane
10 bubbling from Siberian thaw lakes as a positive feedback to climate warming, *Nature*,
11 443(7107), 71–5, doi:10.1038/nature05040, 2006.

12 Walter, K. M., Smith, L. C., and Chapin, F. S.: Methane bubbling from northern lakes:
13 present and future contributions to the global methane budget, *Philos. Trans. A. Math. Phys.*
14 *Eng. Sci.*, 365(1856), 1657–76, doi:10.1098/rsta.2007.2036, 2007.

15 3

16 Walter, K. M., Engram, M., Duguay, C. R., Jeffries, M. O., and Chapin, F. S.: The potential
17 use of Synthetic Aperture Radar for estimating methane ebullition from Arctic lakes, *J. Am.*
18 *Water Resour. Assoc.*, 44(2), 305–315, 2008b.

19 Walter Anthony, K., Vas, D. A., Brosius, L., Chapin III, F. S., and Zimov, S. A.: Estimating
20 methane emissions from northern lakes using ice- bubble surveys, *Limnol. Oceanogr.*:
21 *Methods*, 8, 592–609, 2010.

22 Walter Anthony, K. M., Anthony, P., Grosse, G., and Chanton, J.: Geologic methane seeps
23 along boundaries of Arctic permafrost thaw and melting glaciers, *Nat. Geosci.*, 5(6), 419–426,
24 doi:10.1038/ngeo1480, 2012.

25 Walter Anthony, K. M. and Anthony, P.: Constraining spatial variability of methane
26 ebullition seeps in thermokarst lakes using point process models, *J. Geophys. Res.*
27 *Biogeosciences*, 118, 1-20, doi:10.1002/jgrg.20087, 2013.

28 Walter Anthony, K. M., Zimov, S. A., Grosse, G., Jones, M. C., Anthony, P., Chapin III, F.
29 S., Finlay, J. C., Mack, M. C., Davydov, S., Frenzel, P., and Frolking, S.: A shift of

1 thermokarst lakes from carbon sources to sinks during the Holocene epoch, *Nature*, 511, 452-
2 456, doi: 10.1038/nature13560, 2014.

3 West, J. J. and Plug, L. J.: Time-dependent morphology of thaw lakes and taliks in deep and
4 shallow ground ice, *J. Geophys. Res.*, 113(F1), 1–14, doi:10.1029/2006JF000696, 2008.

5 Wik, M., Crill, P. M., Bastvikenm D., Danielsson, Å., and Norbäck, E.: Bubbles trapped in
6 arctic lake ice: Potential implications for methane emissions, *J. Geophys. Res.*, 116(G3), 1–
7 10, doi:10.1029/2011JG001761, 2011.

8 Tarnocai, C., Canadell, J. G., Schuur, E. A. G., Kuhry, P., Mazhitova, G., and Zimov, S.: Soil
9 organic carbon pools in the northern circumpolar permafrost region, *Global Biogeochem.*
10 *Cycles*, 23(2), 1–11, doi:10.1029/2008GB003327, 2009.

11 Zimov, S. A., Voropaev, Y. V., Semiletov, I. P., Davidov, S. P., Prosiannikov, S. F., Chapin
12 III, F. S., Chapin, M. C., Trumbore, S., and Tyler, S.: North Siberian Lakes: A methane
13 source fueled by Pleistocene carbon, *Science*, 277(5327), 800–802,
14 doi:10.1126/science.277.5327.800, 1997.

15 Zimov, S. A., Davydov, S. P., Zimova, G. M., Davydova, A. I., Schuur, E. A. G., Dutta, K.,
16 and Chapin III, F. S.: Permafrost carbon: Stock and decomposability of a globally significant
17 carbon pool, *Geophys. Res. Lett.*, 33(20), 0–4, doi:10.1029/2006GL027484, 2006.

18
19
20
21
22
23

24 Table 1. Seep density and estimated mean whole-lake ebullition flux of Goldstream L.,
25 Fairbanks, Alaska derived from 2011 and 2012 optical aerial image dataset and from ground
26 surveys. The ground survey estimates are from previously published study by Walter Anthony
27 and Anthony, 2013 and Greene et al., 2014, based on ground surveys conducted over multiple
28 years (2007-2011) at Goldstream L.

Seep Density (seeps m ⁻²)	Mean Whole-Lake Ebullition
---------------------------------------	----------------------------

Prajna Lindgren 9/10/15 10:03 PM
Deleted: [

Prajna Lindgren 9/10/15 10:03 PM
Deleted: ;

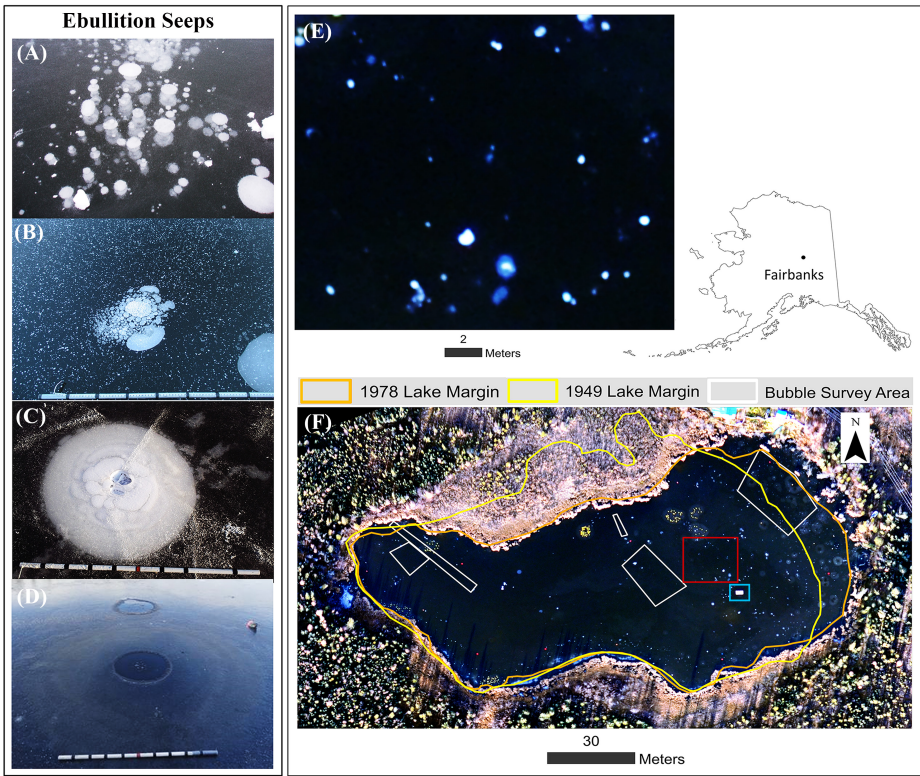
Prajna Lindgren 9/10/15 10:03 PM
Deleted:]

Prajna Lindgren 11/11/15 9:35 AM
Deleted: .

Surveys	A	B	C	Hotspot	All Seeps	(ml gas m ⁻² d ⁻¹)
Aerial (14-Oct-11)	0.026	0.059	0.019	0.017	0.119	174±28
Aerial (13-Oct-12)	0.061	0.083	0.021	0.021	0.185	216±33
Ground surveys	0.366	0.099	0.032	0.011	0.508	170±54

1

2



3

4 **Figure 1.** Photos showing four distinct patterns of point source ebullition seeps in early
5 winter lake ice: (a) A-type; (b) B-type; (c) C-type; (d) Hotspot. The white speckles on the
6 background lake ice surface in (b) are snow/hoar ice crystals, not bubbles; (e) a close-up (red
7 box in the lake image shown in (f)) shows the appearance of ebullition bubble patches as
8 bright white spots on the aerial image (natural color composite of red, green and blue bands)
9 of Goldstream Lake ([64.91°N, 147.84°W](#)), Fairbanks, Alaska acquired on 14 October 2011. A

Prajna Lindgren 9/19/15 11:41 PM

Comment [1]: Table 2 is removed.

Prajna Lindgren 9/19/15 11:39 PM

Deleted: Table 2: Total number of identified bubble patches and comparison between 2011 and 2012. Patch regularity is evaluated by comparing overlap area between bubble patches mapped in 2011 and 2012, assuming that overlapping patches represent the same point-source seep. Total re-appeared bubble patches (%) represent the fraction of total bubble patches mapped that are occurring in the same location in both years.

Prajna Lindgren 9/6/15 10:50 PM

Deleted:

[15]

Prajna Lindgren 11/11/15 9:13 AM

Formatted: English (US)

Prajna Lindgren 11/11/15 9:13 AM

Formatted: English (US)

Prajna Lindgren 11/11/15 9:13 AM

Formatted: English (US)

Prajna Lindgren 11/11/15 9:13 AM

Formatted: English (US)

Prajna Lindgren 11/11/15 9:13 AM

Formatted: English (US)

Prajna Lindgren 11/11/15 9:13 AM

Formatted: English (US)

Prajna Lindgren 11/11/15 9:13 AM

Formatted: English (US)

Prajna Lindgren 11/11/15 9:13 AM

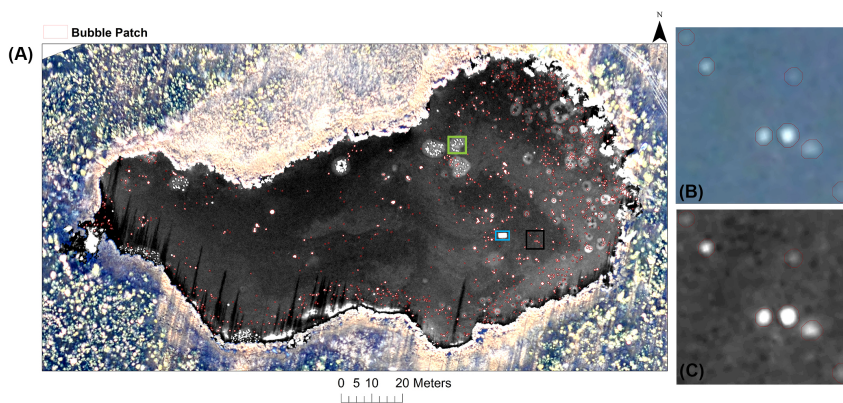
Formatted: English (US)

Prajna Lindgren 11/11/15 9:13 AM

Formatted: English (US)

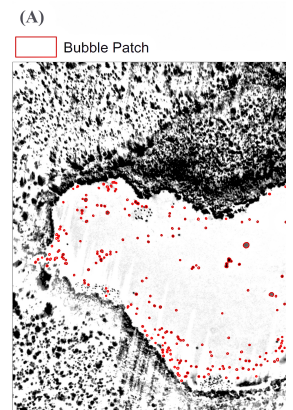
1 rectangular wooden instrument platform (highlighted in blue box) also appears bright.

2



3
4 **Figure 2. (a)** 2011 bubble patch map of Goldstream L. overlaid on Principal Component 1
5 image (PC 1, inverted). The land around lake is shown in true color composite of red, green
6 and blue bands (RGB); (b) and (c) show the area highlighted in the black box in (a) overlaid
7 on RGB composite and PC 1 respectively. Bright bubble patches appear distinct against dark
8 lake ice on PC 1. A rectangular wooden instrument platform in the center of the lake (blue
9 box) as well as clusters of lily pads (one example highlighted in green box) on the northern
10 and south-western parts of the lake (see Fig. 1) also appear bright on PC 1.

Prajna Lindgren 9/9/15 11:10 PM



Deleted:

Prajna Lindgren 11/11/15 9:13 AM

Formatted: English (US)

Prajna Lindgren 9/9/15 11:30 PM

Deleted: (b) and

Prajna Lindgren 9/9/15 11:30 PM

Deleted: c

Prajna Lindgren 9/9/15 11:14 PM

Deleted: PC 1 and true color composite of red, green and blue bands (

Prajna Lindgren 9/9/15 11:32 PM

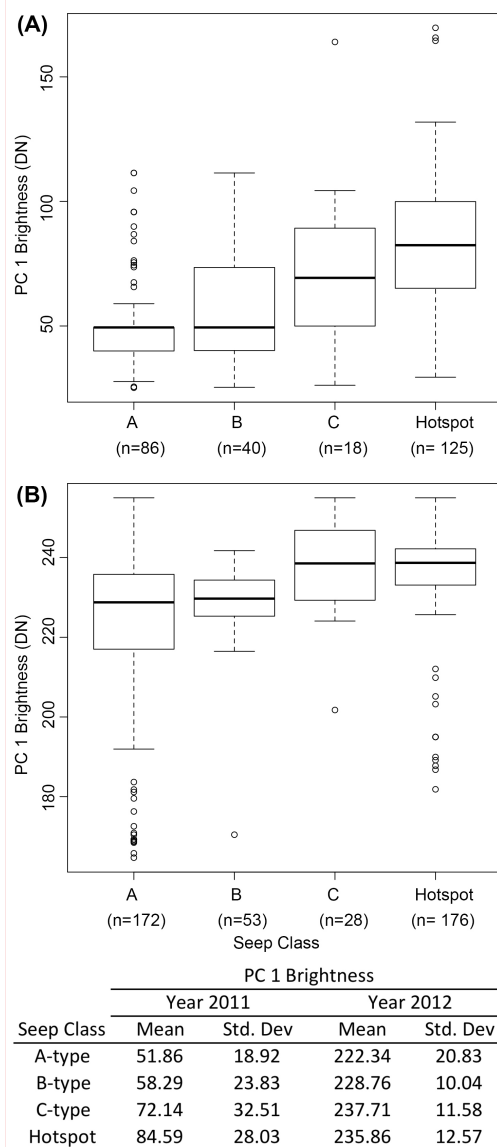
Deleted:)

Prajna Lindgren 9/9/15 11:30 PM

Deleted: Bubble patches appear bright in RGB whereas they appear dark in PC 1.

Prajna Lindgren 9/9/15 11:31 PM

Deleted: dark



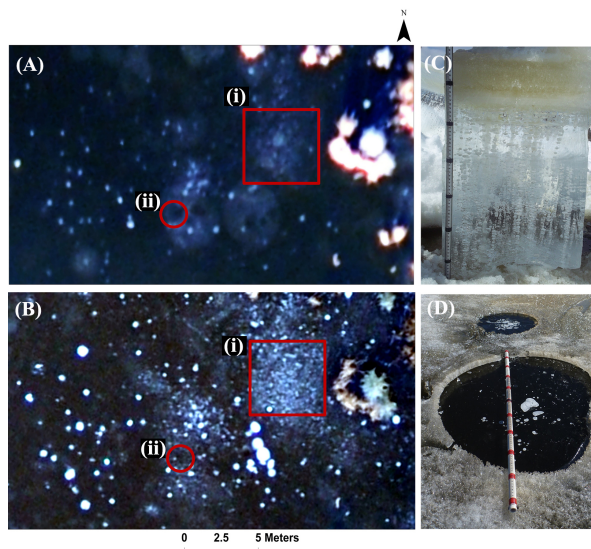
Prajna Lindgren 9/8/15 3:11 PM
Comment [2]: Revised figure. PC 1 brightness is reversed.

1
2 **Figure 3.** Box plots of PC 1 brightness values for bubble patches with different classes of
3 seeps in 2011 (a) and 2012 (b). Significant differences (p-values < 0.05) based on their PC_1
4 mean brightness values were found between C- and A- type seeps, Hotspot and A-type seeps,

Prajna Lindgren 9/6/15 1:07 AM
Deleted: B
Prajna Lindgren 9/6/15 1:07 AM
Deleted: ,
Prajna Lindgren 9/6/15 1:07 AM
Deleted: bubble patches identified in aerial images as

1 and Hotspot and B-type seeps for 2011; and C- and A- type seeps, Hotspot and A-type seeps
 2 for 2012.
 3

Prajna Lindgren 9/10/15 9:28 AM
 Deleted: show significant difference with p-values < 0.05 at the 95% confidence interval



4
 5 **Figure 4. (a-b)** Close-up of low-altitude aerial images from Goldstream L. (~10-15 m from
 6 the eastern thermokarst margin), Fairbanks, Alaska [the same aerial extent shown in (a) –
 7 October 2011; (b) – October 2012]. The red box (i) highlights a densely packed cluster of a
 8 mm-scale ebullition bubbles (Tiny-type seep) in both years. A few B or C-type seeps also
 9 occurred among the Tiny-type ebullition bubbles inside the area marked by the red square.
 10 The red circle (ii) shows an area of Hotspots. In 2011, the Hotspots appear dark similar to
 11 clear black ice surrounded by a bright circular patch, likely hoar frost formed around open
 12 water holes; (c) An ice block cross-section with the Tiny-type seep bubbles in the bubble
 13 cluster area shown in area (i); (d) In April 2012, the Hotspot highlighted in area (ii) seem to
 14 be mostly covered with a very thin layer of fresh black ice with a few bubbles trapped
 15 beneath; however there was a mostly ice-free cavity in the ice above the Hotspots locations
 16 while the rest of the lake ice was still ~ 50 cm thick.
 17

Prajna Lindgren 9/8/15 11:35 AM
 Deleted: fifth class of
 Prajna Lindgren 9/8/15 11:35 AM
 Deleted: seep

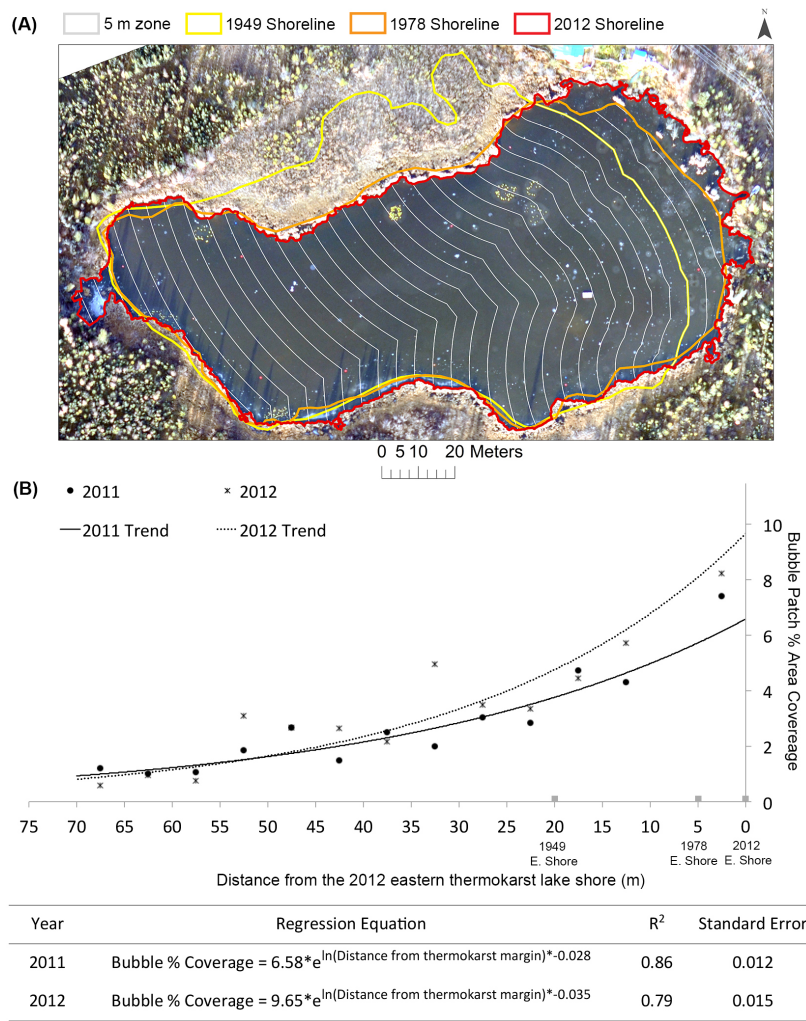


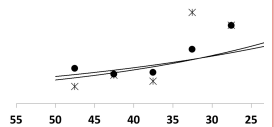
Figure 5. (a) The lake perimeters from 1949 (yellow shoreline), 1978 (orange) and 2012 (red) are overlaid on an aerial image acquired on 14 October 2011. Lake area change between 2011 and 2012 is minimal. The lake is divided in zones of 5 m width (white lines), for which percent bubble patch area was calculated for comparison to the distance from the rapidly expanding eastern lake margin. **(b)** An inverse exponential relationship between bubble patch percent cover and distance from the eastern thermokarst margin of Goldstream L., Fairbanks, Alaska.

Prajna Lindgren 9/9/15 4:35 PM

(A)

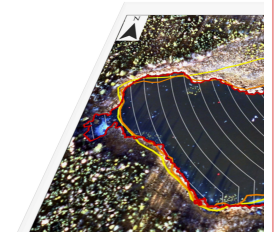
• 2011 × 2012

5 m wide zone
1949 Lake Margin
1978 Lake Margin
2012 Lake Margin



(B)

Distance fro



Deleted:

Prajna Lindgren 9/9/15 4:42 PM

Moved (insertion) [6]

Prajna Lindgren 9/9/15 4:42 PM

Deleted: An inverse exponential relationship between bubble patch percent cover and distance from the eastern thermokarst margin of Goldstream L., Fairbanks, Alaska;

Prajna Lindgren 9/9/15 4:42 PM

Moved up [6]: The lake perimeters from 1949 (yellow shoreline), 1978 (orange) and 2012 (red) are overlaid on an aerial image acquired on 14 October 2011. Lake area change between 2011 and 2012 is minimal. The lake is divided in zones of 5 m width (white lines), for which percent bubble patch area was calculated for comparison to the distance from the rapidly expanding eastern lake margin.

Prajna Lindgren 9/9/15 4:42 PM

Deleted: The lake perimeters from 1949 (yellow shoreline), 1978 (orange) and 2012 (red) are overlaid on an aerial image acquired on 14 October 2011. Lake area change between 2011 and 2012 is minimal. The lake is divided in zones of 5 m width (white lines), for which percent bubble patch area was calculated for comparison to the distance from the rapidly expanding eastern lake margin. [16]

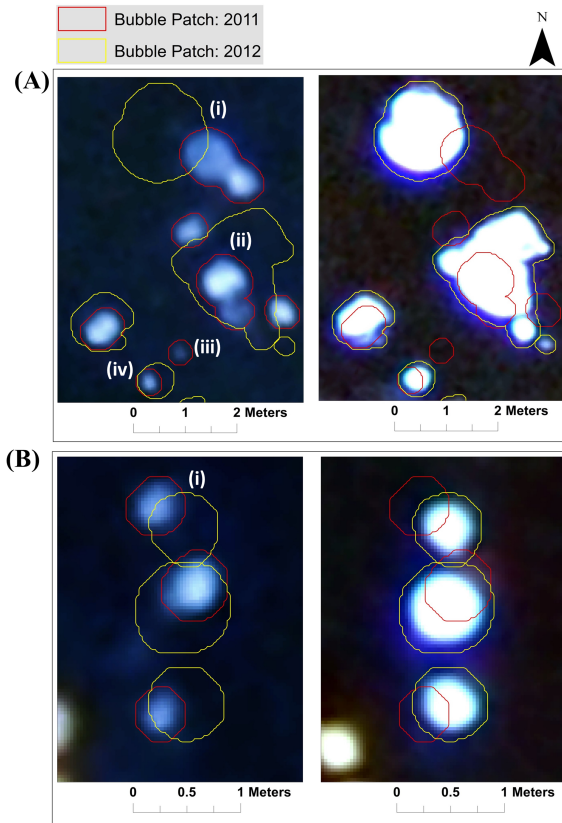


Figure 6. Comparison of bubble patches visible in thin lake ice two days after freeze-up in October 2011 (left-side images) and four days after freeze-up in October 2012 (right side images). Image pairs in a and b represent the same locations in 2011 and 2012. Four major characteristics of bubble patches are identified in panel a: (i) Bubble patches may shift up to 50 cm in location (geolocation error < 20 cm) in non-consistent directions; (ii) Bubble patch size and morphology varies between years during the first few days following freeze-up; (iii) Bubble patches visible during the first few days of freeze-up in one year are not visible during the first few days of freeze-up in another year; and (iv) Bubble patches are similar in shape but not in size. Panel b shows another example of horizontal shift of bubble patches (i).

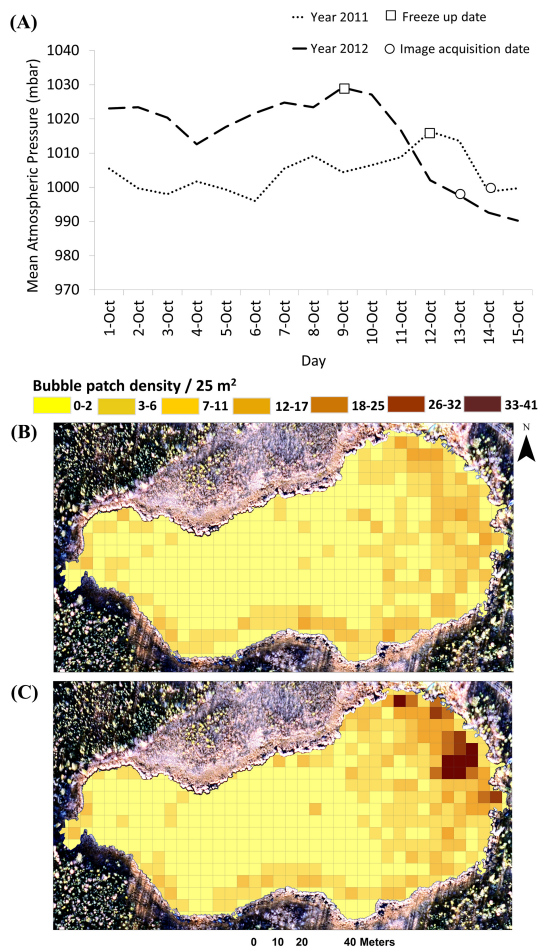


Figure 7. In (a) The graph of mean daily atmospheric pressure (mbar) observed between 1-15 October in 2011 and 2012 shows that the magnitude of atmospheric pressure drop prior to image acquisition was twice as high in 2012 and 2011; pressure drops are known to induce ebullition. Bubble patch density in a 5 x 5m grid as seen in the October images of the year (b) 2011; and (c) 2012. Generally darker grid cell colors in panel suggest a higher density of seeps in 2012 compared to 2011, which is consistent with (1) a two-times longer period of ice formation (four days in 2012 vs. two days in 2011) for bubbles to accumulate and (2) atmospheric pressure patterns. Spatial distribution of bubble patches clearly shows a higher concentration of methane emission along the rapidly expanding eastern thermokarst margin in both years.

Prajna Lindgren 9/24/15 12:17 PM

Comment [3]: Revised figure. Panels are reversed.

Prajna Lindgren 9/8/15 3:15 PM

Moved (insertion) [5]

Prajna Lindgren 9/8/15 3:16 PM

Deleted: c

Prajna Lindgren 9/8/15 3:17 PM

Deleted: Generally darker grid cell colors in panel suggest a higher density of seeps in 2012 compared to 2011, which is consistent with (1) a two-times longer period of ice formation (four days in 2012 vs. two days in 2011) for bubbles to accumulate and (2) atmospheric pressure patterns.

Prajna Lindgren 9/8/15 3:16 PM

Deleted: a

Prajna Lindgren 9/8/15 3:16 PM

Deleted: b

Prajna Lindgren 9/8/15 3:15 PM

Moved up [5]: In (c) The graph of mean daily atmospheric pressure (mbar) observed between 1- 15 October in 2011 and 2012 shows that the magnitude of atmospheric pressure drop prior to image acquisition was twice as high in 2012 and 2011; pressure drops are known to induce ebullition. Generally darker grid cell colors in panel suggest a higher density of seeps in 2012 compared to 2011, which is consistent with (1) a two-times longer period of ice formation (four days in 2012 vs. two days in 2011) for bubbles to accumulate and (2) atmospheric pressure patterns.

Prajna Lindgren 9/8/15 3:17 PM

Deleted: ;

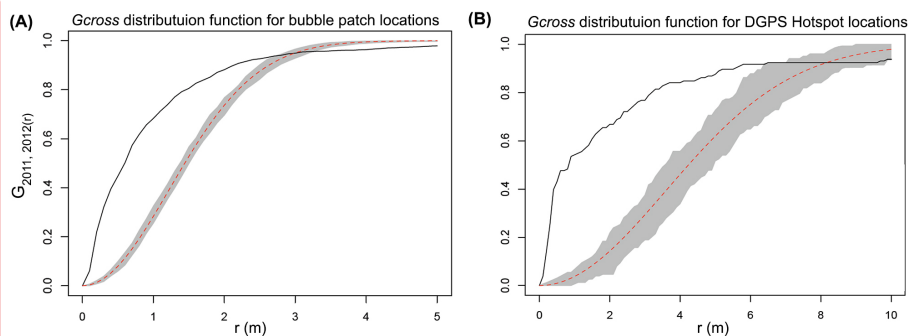


Figure 8. Cumulative distribution function of distances (r) between seeps identified in two different years 2011 and 2012. The black line shows actual observed data and red line shows the theoretical expected value assuming the points are completely random. Gray shaded area shows a theoretical seep distance function for a random seep distribution (95% confidence band). The deviation between the observed empirical value (black curve) and theoretical expected value (red curve) suggests that a large and statistically significant number of seeps show spatial dependence between years 2011 and 2012. (a) Distance function for bubble patches derived from image dataset. The actual curve is well above the theoretical curve over separation distances of 0-2 meter and thus a statistically significant number of second year bubble patch center points are less than 2 meters away from the first year center points. The actual curve is below the theoretical curve at the top after 3 meter distance separation suggesting that there are far less number of seeps at large distances; (b) Distance function for seeps derived from DGPS field-measured Hotspots. The observed function for the DGPS Hotspot locations rises almost vertically over separation distances of 0-1 meter deviating away from the theoretical function, i.e. a statistically significant number of Hotspot seeps did not move much from the first year location.

Prajna Lindgren 9/24/15 7:44 PM

Comment [4]: Revised figure.

Prajna Lindgren 9/6/15 12:22 PM

Moved (insertion) [4]

Prajna Lindgren 9/6/15 12:54 PM

Deleted: The black line shows actual observed data.

Prajna Lindgren 9/6/15 12:24 PM

Deleted: seeps

Prajna Lindgren 9/6/15 12:22 PM

Moved up [4]: Gray shaded area shows a theoretical seep distance function for a random seep distribution (95% confidence band). The black line shows actual observed data.

Prajna Lindgren 9/6/15 12:10 PM

Deleted: The measured data indicate that a much larger proportion of the seep distances is closer than expected for a random seep distribution, suggesting statistically significant stability in seep locations over time.

1 Supplementary

2 **Text S1. Principal Component Analysis**

3

4 Multi-spectral remote sensing data consists of high inter-band correlation and therefore
5 bands within a dataset carry redundant information (Rocchini et al., 2007). Principal
6 Component Analysis (PCA) transforms a set of correlated variables in original image bands
7 into a set of linearly uncorrelated orthogonal components (principal components)
8 (Schowengerdt, 2007; Estronell et al., 2013). It reduces the dimensionality of the data and
9 outputs the maximum amount of information with a physical meaning from the original
10 bands into the least number of principal components (Estronell et al., 2013). After
11 transformation, the first principal component has the variables that account for the most
12 variance in the dataset and each succeeding independent component in turn carries less and
13 less of the original data variance.

14

15 **Text S2. Image segmentation and classification to map bubble patches on lake ice image**

16

17 Based on empirical performance tests, we used the first two PCA components (PC 1 and PC
18 2) to perform multi-resolution segmentation embedded in eCognition Developer™ software
19 to create image objects (eCognition Developer 7 Reference, 2007a). The advantage of using
20 multi-resolution segmentation is that it allows to create objects of different scales while
21 minimizing the heterogeneity within the resulting object at the given scale (Baatz and
22 Schape, 2000). For example, we applied a large-scale factor to create large objects of
23 different lake ice characteristics and a small-scale factor to create small bubble patch objects.
24 We performed region-specific classification for the identification of target features within the
25 domain of that particular region. In general, for classification we used spectral characteristics
26 in PC bands 1 and 2, contextual information pertaining to image objects such as an image
27 object's relationship with its neighbors and sub- and super-objects, a Canny edge detection
28 algorithm (Canny, 1986; eCognition Developer 7 Reference, 2007b) and morphological
29 filters available in the eCognition Developer™ software.

30

Prajna Lindgren 11/11/15 1:47 PM

Comment [5]: Text S1-S3 are added

The classification method performed very well in identifying bubble patches (Fig. 2) with an overall accuracy of 98% when compared to manually identified bubble features in image segments that served as our ground truth sample data for classification accuracy assessment. Due to thin lake ice condition on image acquisition days, it was not feasible to collect ground truth data of ebullition bubble patches for the purpose of accuracy assessment. It is important to note we did not check our classification accuracy in terms of object's geometry or boundary delineation. We only performed quantitative site-specific accuracy assessment using error matrix that only checks the agreement of object classes between manually classified reference sample and object-based classification results.

Text S3. Classification of bubble patches based on size

The Maximum Likelihood Classification (MLC) was a pixel-based classification that categorized bubble patches based on the pixel spectral characteristics. Therefore, the pixels within an extended bubble patches may be assigned to more than one seep class (multi-type bubble patch) depending on the variation of brightness values within the patch. Since the size of bubble patches is also an additional important indicator of seep class and methane flux (Walter Anthony et al., 2010), in a subsequent step we further investigated the size of each seep class in a multi-type bubble patch identified by MLC. Based on the highest flux seep type and its size in a patch, we re-assigned bubble patches to a more accurate methane flux. For example, a bubble patch with a combination of C-, B- and A-type seep, C-type is the highest flux seep. Thus, we checked the total area of C-type seep. The whole bubble patch was classified as C-type seep only if the area of C-type seep was greater than 0.04 m² otherwise it was classified as B-type seep (Table S1). The thresholds on size are based on seep morphology described by Walter Anthony et al., 2010 and our field observations.

Table SI. Conditions applied to classify bubble patches that are identified to have multiple seeps (multi-type bubble patch) by MLC. A single final seep type is assigned to the multi-type bubble patch based on the size of the highest flux seep that is present in the patch.

Highest flux seep in the bubble patch									
	Hotspot				C-type seep		B-type seep		
If area (m ²)	< 0.04	0.04 >=		< 0.09	>= 0.09	< 0.04	>= 0.09	< 0.01	0.01
Assign class	B-type	C-type		Hotspot		B-type	C-type	A-type	B-type

Prajna Lindgren 11/11/15 1:46 PM

Comment [6]: New table. Tables are before figures in this revised version.

Table S2. Tukey's Honestly Significant Difference (HSD) test showing significant difference (with p-values* < 0.05) between bubble patches identified in aerial images as C- and A- type seeps, Hotspot and A-type seeps, and Hotspot and B-type seeps for 2011 and 2012.

Year 2011

95 % Confidence Interval				
Seeps	Mean Difference	Lower Bound	Upper Bound	p-values
B-A	-6.43	-18.89	6.03	0.54
C-A*	-20.28	-37.14	-3.40	0.01*
Hotspot-A*	-32.73	-41.85	-23.61	0*
C-B	-13.84	-32.32	4.63	0.21
Hotspot-B*	-26.30	-38.13	-14.48	0.00*
Hotspot-C	-12.45	-28.87	3.95	0.21

Year 2012

95 % Confidence Interval				
Seeps	Mean Difference	Lower Bound	Upper Bound	p-values
B-A	-6.41	-12.95	0.13	0.06
C-A*	-15.36	-23.84	-6.88	0.00*
Hotspot-A*	-13.51	-17.98	-9.05	0.00*
C-B	-8.95	-18.67	0.78	0.08
Hotspot-B*	-7.10	-13.62	-0.58	0.02*
Hotspot-C	1.85	-6.62	10.31	0.94

Table S3: Accuracy assessment table for bubble patch classification

Prajna Lindgren 11/11/15 1:46 PM

Comment [7]: New table

Seep Class	Year	Producer's Accuracy (%)	Omission Error (%)	Commission Error (%)	User's Accuracy (%)	Overall Accuracy
A-type	2011	50.00	50.00	38.46	61.54	38.10
	2012	52.54	47.46	6.06	93.94	50.82
B-type	2011	71.43	28.57	61.54	38.46	33.33
	2012	63.64	36.36	70.21	29.79	25.45
C-type	2011	33.33	66.67	75.00	25.00	16.67
	2012	10.00	90.00	92.86	7.14	4.35
Hotspot	2011	45.83	54.17	8.33	91.67	44.00
	2012	67.50	32.50	27.03	72.97	54.00

Figure S1. Image object hierarchy used in the objected oriented classification technique developed to identify bubble patches on early winter lake ice. Image segmentation is performed in each level and image objects are classified. In the first level, segmentation is performed on the whole lake image to identify Lake Shore and Lake. In the second level, only the Lake region is segmented and image objects derived from the Lake are classified into different lake ice characteristics. This process continues as it proceeds towards lower and finer classification levels until Bubbles are identified in the lake ice.

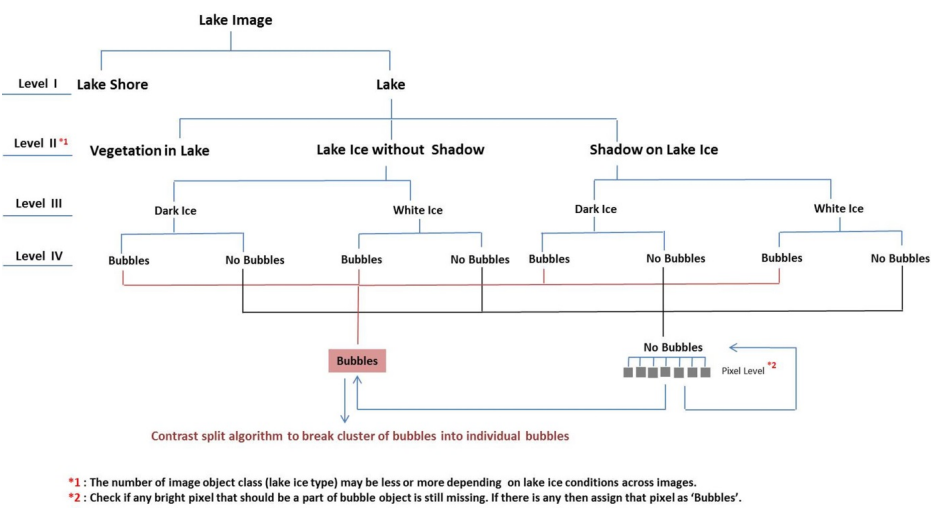


Figure S2. (a) and (b) are 2011 bubble patch maps of Goldstream L. overlaid on Principal Component 1 image (PC 1) and inverted PC 1. Inverted PC 1 is calculated using the formula $\text{Inverted PC 1} = 255 + (\text{PC 1} * (-1))$. The land around lake is shown in true color composite of red, green and blue bands (RGB); (c) and (d) show the area highlighted in the black box in (a) overlaid on RGB composite and PC 1 respectively. Bubble patches appear bright in RGB whereas they appear dark in PC 1. A rectangular wooden instrument platform in the center of the lake (blue box) as well as clusters of lily pads (one example highlighted in green box) on the northern and south-western parts of the lake (see Fig. 1) also appear dark on PC 1. Therefore, we inverted PC 1 to retain their original brightness characteristic, i.e. appear bright against background lake ice. This is shown in (e).

Prajna Lindgren 11/11/15 1:46 PM
Comment [8]: New figure.

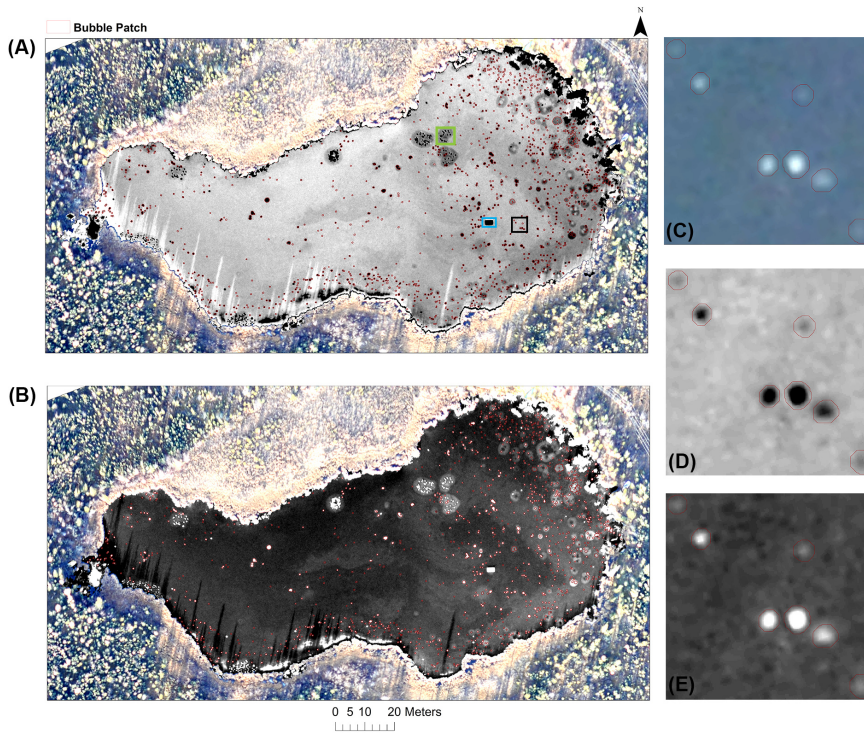


Figure S3. Photo of an ice block cross-section in April of 2013 from an ebullition seep on Goldstream L., Fairbanks, Alaska. The bubble size variation traces dynamics of the point source emission during winter. Vertically-oriented, circular and flat layers of methane bubbles separated by clear ice indicate highly episodic nature of ebullition. Varying size of bubbles and periods of ice growth with no bubbling confirm previous bubble-trap observations that bubbling is episodic rather than constant over time. Black marks on the ruler have 10-cm spacing.

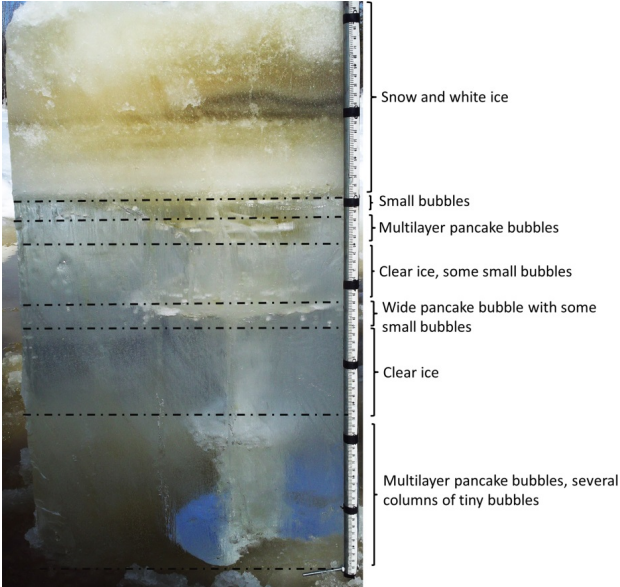


Figure S4. Ice-free Hotspot location map of Goldstream L. overlaid on a natural color composite (red, green and blue bands) image acquired using a UAV on 14 October, 2012.

